FACULTY OF SCIENCE

Complementarity of high energy and high intensity experiments for dark photon benchmarks

Author: Josh Greaves

Thesis submitted for degree: Master Programme in Physics, General
Project duration: 1 semester equivalent / 30 Credits
Division of Particle Physics

Supervised by Caterina Doglioni, Philip Harris, Katherine Pachal

Complementarity of high energy and high intensity experiments for dark photon benchmarks

Author Josh Greaves

Degree Master Programme in Physics, General

Supervisor Caterina Doglioni

ABSTRACT

Physical phenomena that are unexplained by the Standard Model (SM) of particle physics, are the subject of the area of research known as physics Beyond the Standard Model (BSM). BSM physics contains many Dark Matter (DM) theories which have emerged; from particles such as axions, neutrinos, and Weakly Interacting Massive Particles (WIMPs), to primordial black holes and others. The range of experiments at the frontiers of research are equipped to probe model parameter space with different sensitivites. The energy frontier, exemplified by the Large Hadron Collider (LHC), reaches the TeV energy scale and beyond. The intensity frontier looks for rare processes and precision deviations. The cosmic frontier searches astrophysical data. Some rely on invisble signatures, and some require visible SM decays of DM. There is a great deal of experimental complementarity, and cross-frontier collaboration needs to be prioritized.

Minimal WIMP based models within the reach of current experiments are presented. The model benchmarks allow for the comparison of limits on the ability to constrain model parameters, to be made between experiments.

These limits can be scaled between different couplings within a model, or even between models, provided that only the cross section varies and is known in each case. Limits set for more general vector models could be scaled to dark photon limits, the possibility of which is discussed. The acceptances are confirmed to be the same between the two models considered in this paper. Thermal relic bounds are also imposed, and comparisons are made for each model in an appropriate plane on the y-axis known as the *yield parameter*. In addition, a heat map approach to plotting the Dark Matter and mediator masses is presented, with a focus on the minimum coupling limit imposed by the relic density. This approach facilitates visualization on one plot the viable regions of mass-mass parameter space in order not to overproduce DM, for each model considered. A brief outlook is given on the current state of cross-frontier collaboration, in a number of efforts, all with the aim of exploiting complementarity in DM searches.

FYSM30 - Particle Physics Dept. CONDUCTED: Winter 21 - Spring 22

Abstract

Physical phenomena that are unexplained by the Standard Model (SM) of particle physics, are the subject of the area of research known as physics Beyond the Standard Model (BSM). BSM physics contains many Dark Matter (DM) theories which have emerged; from particles such as axions, neutrinos, and Weakly Interacting Massive Particles (WIMPs), to primordial black holes and others.

The range of experiments at the frontiers of research are equipped to probe model parameter space with different sensitivites. The energy frontier, exemplified by the Large Hadron Collider (LHC), reaches the TeV energy scale and beyond. The intensity frontier looks for rare processes and precision deviations. The cosmic frontier searches astrophysical data. Some rely on invisble signatures, and some require visible SM decays of DM. There is a great deal of experimental complementarity, and cross-frontier collaboration needs to be prioritized.

Minimal WIMP based models within the reach of current experiments are presented. The model benchmarks allow for the comparison of limits on the ability to constrain model parameters, to be made between experiments.

These limits can be scaled between different couplings within a model, or even between models, provided that only the cross section varies and is known in each case. Limits set for more general vector models could be scaled to dark photon limits, the possibility of which is discussed. The acceptances are confirmed to be the same between the two models considered in this paper.

Thermal relic bounds are also imposed, and comparisons are made for each model in an appropriate plane on the y-axis known as the *yield parameter*. In addition, a heat map approach to plotting the Dark Matter and mediator masses is presented, with a focus on the minimum coupling limit imposed by the relic density. This approach facilitates visualization on one plot the viable regions of mass-mass parameter space in order not to overproduce DM, for each model considered.

A brief outlook is given on the current state of cross-frontier collaboration, in a number of efforts, all with the aim of exploiting complementarity in DM searches.

Acknowledgments

For the time they made for me out of their busy schedules, having never worked with or met with me before, I thank Kate Pachal and Phil Harris of the EF10 group; the assistance and guidance they gave me was an enormous help.

My supervisor Caterina agreed to be my supervisor at a fairly inopportune period for her, for which I am truly grateful. I could not have been part of this effort, from which I have learned and benefited a huge amount, had she not made it possible.

I am also thankful to those who made time for me along the way at various sticking points: Ruth Pottgen for assistance in tabulating experiments; Taylor Gray for her back and forth with me on MadGraph model implementation; the LDMX group for including me in their weekly discussions; the rest of the EF10 group; and the Particle Physics Division at Lund.

This project was also part of the group supported by the Knut and Alice Wallenberg Foundation at Lund University, which also includes LDMX.

Abbreviations

SM	Standard Model
QED	Quantum Electro Dynamics
QFT	Quantum Field Theory
LHC	Large Hadron Collider
CoM	Centre of Mass
BSM	Beyond Standard Model
CP	Charge-Parity(symmetry)
QCD	Quantum Chromo Dynamics
WIMP	Weakly Interacting Massive Particle
CMBR	Cosmic Microwave Background Radiation
SLAC	Stanford Linear Accelerator Center
FCC	Future Circular Collider
P5	Particle Physics Project Prioritization Panel
iDMEu	Initiative for Dark Matter in Europe and beyond
LOI	Letter Of Intent
DMWG	LHC Dark Matter Working Group
EFT	Effective Field Theory
MSSM	Minimal Supersymmetric Standard Model
NC	Neutral Current
MC	Monte Carlo
LO	Leading Order
NLO	Next to Leading Order
HL-LHC	High Luminosity LHC
ESCAPE	European Science Cluster of Astronomy and Particle physics research

Contents

1 Introduction

1.1 The Standard Model

'Extremely successful' would be a valid way to describe the predictions made by the current physical model of fundamental elementary particles and their interactions: the *Standard Model* (SM).

All known matter is made up of *fermions*, which have half integer spin and obey Fermi-Dirac statistics. This means that they obey the Pauli exclusion principle; one fermion cannot occupy the same quantum state as another. Fermions interact by exchange of *bosons*; particles with integer spin, which obey Bose-Einsten statistics and are able to occupy the same quantum state. Nature's fundamental forces are mediated by Bosons.

The list of fermions is comprised of *Quarks* and *Leptons*, each of which contain six *flavours*. The whole set of SM particles is shown in Figure 5.1 in Appendix A. The list of bosons includes *gauge* bosons with spin one, and scalar bosons with spin zero. The only known scalar boson currently is the Higgs boson, which is the excitation of the Higgs field, responsible for breaking electroweak symmetry, and endowing the weak interaction bosons with mass.

The fundamental interactions of the SM, in decreasing order of coupling strength, and at energies below electroweak symmetry breaking, are: the strong force of Quantum Chromo Dynamics (QCD), which is mediated by the massless gluons between quarks, and also between gluons themselves; the electromagnetic interaction mediated by the photon, which is described completely by Maxwell's equations; the weak interaction mediated by three massive bosons, $W^{\pm}$ and Z^0, which can cause quarks to change flavour. Above the energy of electroweak symmetry breaking, the latter two forces are unified into one fundamental force, characterised by three W bosons and the B boson. The Higgs mechanism is responsible for breaking this symmetry, resulting in the SM photon and the Z^0, which are mixtures of the W^0 and the B states. The remaining W's become the $W^{\pm}$ of the weak interaction.

Notably absent is the weakest force; gravity. Any particle nature of gravity currently lies beyond the Standard Model.

1.2 Beyond the Standard Model

Successful though it is, the SM has proven itself ultimately incomplete. The relentless confirmation of the model's predictions since its origins in the mid 50's, has served to consistently validate the SM. But it is not perfect.

The term was supposedly first coined in *Physical Review Letters* in 1975[1] (though it has also been claimed, by Steven Weinberg[2], that he used it a couple of years earlier). However, the origins of the model stretch back to earlier in the century; perhaps to 1954 when Yang and Mills proposed an extension of gauge theory from Quantum Electro Dynamics (QED) in order to explain the strong interaction [3]. Perhaps even to decades before that, when Quantum Field Theory (QFT) first began to emerge.

Arguably the SM's most famous recent success was the discovery of the Higgs particle in 2012; first postulated by Peter Higgs in 1964[4]. This successful observation was dependent on a particle collider such as that available at the LHC, able to reach the necessary Centre of Mass (CoM) energy and integrated luminosity required to discover the Higgs boson. After more than half a century of being a theorized member of the SM, the Higgs was finally solidified among the other observed particles in the model.

Another demonstration of the model's competence, is the remarkable agreement between the SM prediction of the electron magnetic dipole moment, arising from the spin and charge of the electron[5], and its experimental measurement[6], to within one part per trillion.

As is very well known, the Standard Model is not a complete theory of nature. It is deficient in its ability to answer a number of questions that nature has posed. Models that can explain these deficiencies are described under the catch all term of physics Beyond Standard Model (BSM), and a prominent aspect of BSM physics is the subject of this work.

Among many other features of our universe not explained by the SM, such as the asymmetry between matter and anti-matter[7], neutrino masses[8], the anomalous magnetic moment of the muon[9], and the mystery of Charge-Parity (CP) symmetry preservation within Quantum Chromo Dynamics (QCD)[10], the largest discrepancy between SM theory and experimental observation is probably its inconsistency with general relativity; Einstein's general theory of gravitation. This description of gravity surpassed the accepted mathematics of Newton, and though the SM lacks any particulate or quantum field description of gravity[11], general relativity continues to prove itself as the best model for gravitational interaction.

Along with the success and reliability of general relativity in explaining cosmological observations; from the prediction and recent imaging of black holes[12], to the prediction and measurement of gravitational waves by the Laser Interferometer Gravitational-wave Observatory (LIGO)[13], gravity has also indicated to us that the majority of matter in the universe is not any part of the Standard Model at all. Without any electromagnetic illumination, it appears to interact only gravitationally; hence the name Dark Matter.

1.3 Dark Matter

Cosmological observations point to the existence of Dark Matter as a gravitationally interacting material. In 1933, Fritz Zwicky observed anomalous behaviour among the Coma cluster of galaxies[14]. In Newtonian mechanics, the virial theorem relates the time averaged kinetic energy of a mechanical system of particles, such as stars in a galaxy, to a common central force such as gravity, defined by the gravitational potential.

The total gravitational potential energy in the Coma cluster is determined by its total constituent mass. Zwicky discovered, from the redshift of galaxies toward the cluster's edge, that the average velocities exceeded those predicted by the theory. He concluded that there must be some mass hidden from view, which he called *dunkle materie*, or "Dark Matter". Even earlier than Zwicky's work, in 1930, the Swedish astronomer Knut Lundmark had concluded that additional mass was required to explain galactic rotation curves, even calling it 'dunkle materie'. However, this would unfortunately be lost to history, leading to Zwicky being recognised as the pioneer of the term. This may be partly due to the fact that Lundmark stopped short of suggesting it may be a new kind of matter.

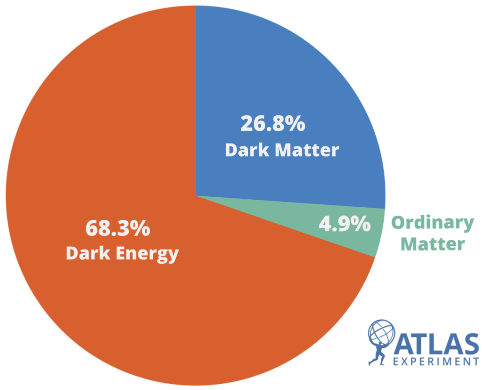

Figure 1.1: Estimated matter-energy content of the universe.[15][16]

Based on the stellar velocities, this unseen matter must be contributing the majority of the galactic mass to the cluster. The current estimate (c. 2013 [16]) is that Dark Matter comprises approximately 26.8% of the total energy density of the universe, and matter 4.9%; a ratio of $\approx 5.5 : 1$. The remainder is Dark Energy; a separate phenomenon which accounts for the accelerated expansion of the universe.

Zwicky's Dark Matter observations were reinforced by Vera Rubin and Kent Ford in the 1970's, when they measured the orbital speeds of spiral galaxies, which became known as the Galaxy rotation problem[17]. It's a problem because the orbital velocities would be expected to decrease with radius, as the luminous matter density decreases, since the concentration of luminous matter is highest toward the centre of a galaxy. Contrary to expectation, the outer star velocities were measured to be just as high as stars closer to the luminous centre; much higher velocities than expected, and too large for the galaxies to remain intact as they were, demonstrated in Fig. 1.2. Rubin and Ford concluded that the observed surplus of gravitational potential implied an approximate six to one ratio of dark mass to luminous mass. This Dark Matter concentration is distributed in a region that spreads far beyond the boundary of the visible galactic matter, often referred to as a *Dark Matter Halo*.

Further confirmation of this extra galactic mass came in the form of gravitational lensing measurements (see Fig. 1.3). As spacetime curves due to the presence of mass, the paths of light also become curved in this so called lensing effect around massive objects.

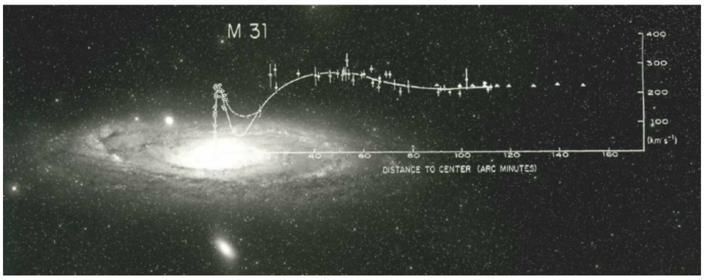

Figure 1.2: Mean radial velocities of the M31 galaxy superimposed on the image from Palomar Sky Survey. Triangles indicate velocities from radio observations. Rotation velocity remains flat beyond the visible region which implies that the total mass is increasing with radius, indicating Dark Matter presence.[18]

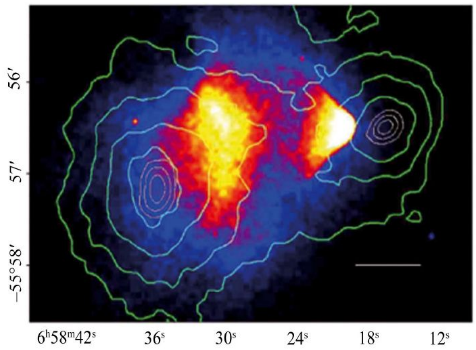

Figure 1.3: Image of 1E 0657-558 'bullet' cluster in X-ray. Color map shows the visible baryonic mass, which is misaligned with the green contours, which show the mapping of the actual gravitational centres according to lensing measurements.[19]

This provides a method to measure the curvature, and therefore the gravitational mass, of an intervening object like a galaxy, which has shown the same discrepancy between luminous and non luminous Dark Matter[20]. All that is currently known about Dark Matter is from gravitational evidence and related astrophysical observations. While Dark Matter is not (yet) a member of the Standard Model of particle physics, it is an accepted component of the standard cosmological model.

1.4 Experiments

The experiments most relevant to this thesis are primarily the Compact Muon Solenoid (CMS)[21] at the LHC[22], and the Light Dark Matter Experiment (LDMX)[23], which is undergoing its first beam testing at the LHC at the time of writing.

ATLAS[24], or 'A Toroidal LHC Apparatus', is an experiment designed to exploit the full potential for discovery at the LHC at CERN. The LHC, currently the world's highest energy particle collider, was built from 1998 to 2008 when it first started up. The 27km ring of superconducting magnets is used to accelerate beams of charged particles in opposite directions, steered toward four collision points, each of which are surrounded by sensitive detector material. Along with ATLAS and CMS, the other experiments are LHCb(beauty)[25], and A Large Ion Collider Experiment (ALICE)[26]. ATLAS measures the output of collisions, and is sensitive to the primary signature of Dark Matter discussed in this work; missing transverse momentum in the presence of an energetic monojet [27]. ATLAS is complemented by CMS measurements, which has similar sensitivity [28].

LHCb and ALICE are not strictly relevant for Dark Matter searches in the context of this paper. ALICE, as the name suggests, uses heavy ion beam collisions such as lead-lead nuclei to focus on Quark Gluon Plasma (QGP), which relates to the physics of the strong interaction. LHCb focuses on bottom-quark or beauty-quark physics, which is distinctive because b-quarks are significantly heavier than all other quarks except top quarks. Their transitions to other flavours are also heavily suppressed, which gives them a distinctive lifetime and allows for *b-tagging* of collision event products. LHCb is used to study CP violation which is inherent in B-meson decays.

LDMX is a smaller scale experiment than ATLAS, consisting of a very precisely tracked electron beam impacting on a fixed tungsten target. While it is undergoing beam tests at CERN at the time of writing, it will conduct its future data taking at the Stanford Linear Acclerator Center (SLAC); its final operating location. According to the report [23], each 'bunch' of electrons consists of only one or two electrons, delivered at a rate of approximately 40 MHz, corresponding to one every 20ns, and the beam energy ranges from 4 - 16 GeV. If an invisible Dark Matter mediator is produced, the electron will recoil with a corresponding quantity of transverse momentum, leading to a missing energy signal in the detector. This experiment is complementary to ATLAS because of its high luminosity, sensitivity to lower couplings and its resulting ability to probe rarer interactions.

1.5 Research frontiers and complementarity

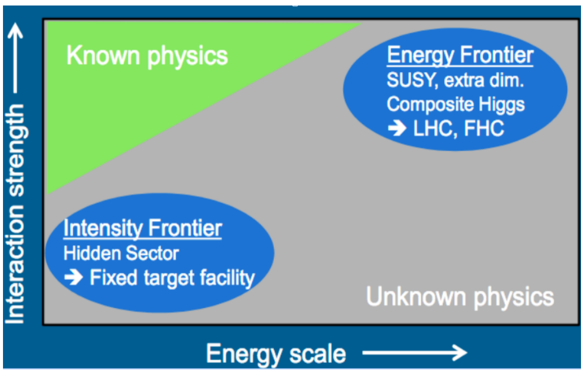

Figure 1.4: Physics reach and complementarity between intensity and energy frontiers.[29]

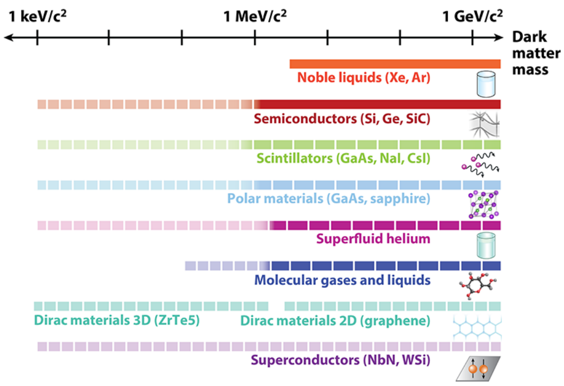

Figure 1.5: Sub-GeV Dark Matter detection sensitivity by material. Solid lines represent current experiments, dashed lines represent materials being considered for future experiments; greyed out lines are long term considerations. [30]

The separate experimental *frontiers* of particle physics research, which is a categorization established by the *Snowmass*[31] community, are configured to probe different but complementary areas of parameter space (Figure 1.4). *Parameter space* refers to the complete set of parameter value combinations which define a specific model. For example, all combinations of mass and coupling values which are free parameters in a model, define the parameter space of that model. Experimental reach within this space is limited, and to probe a range of parameters requires experiments from different frontiers, with different capabilities. Prominent examples of these frontiers are:

- Energy frontier: Colliders such as the LHC can detect processes at the TeV energy scale and beyond. A future example is the *Future Circular Collider (FCC)*[32] .

- Intensity frontier: Rare processes and deviations in precision measurements are accessible to experiments in this category, for example accelerators with fixed targets such as LDMX.

- Cosmic frontier: Conducting experimentation without the need of a man made accelerator, the cosmic frontier probes astrophysical and cosmological data to potentially detect Dark Matter directly (See *Direct Detection*).

Detection strategies for DM are designed differently by each frontier. Characteristics of Dark Matter behaviour at a collider experiment can vary, producing different kinds of visible or invisible signals (see Fig 1.6). At higher energies, heavier particles such as the Higgs can be produced, but lighter or much more weakly coupled particles are harder to detect. Experiments with higher intensity beams allow for the probing of feebler couplings and rarer processes than the energy frontier. Cosmic frontier experiments can then complement these by detecting naturally occurring Dark Matter interactions from the cosmos, confirming any Dark Matter observations made within experiments from the other frontiers. Experimental methods to cover all possibilities fall into four main categories:

- Direct detection: Primarily occuring underground, direct detection experiments aim to directly measure elastic or inelastic interactions with DM (Fig. 1.6 b). Measuring the elastic recoil energy from a nuclear collision is more challenging at low DM mass. Available sources such as Dark Matter Halo particles typically move at non relativistic speeds. Recoil measurements are done by measuring the angle of a recoiling particle's track in a detector, so low mass DM particles have kinetic energy too low for the recoil to be measured. Inelastic interactions can be more sensitive by the use of scintillation or ionization methods. See Figure 1.5 [30] for examples of detection materials.

- Indirect detection: Measurement of the possible Dark Matter annihilation to SM model particles (Fig. 1.6 a). Cosmic frontier examples include the observation of satellite galaxies of the Milky Way by the Fermi Large Area Telescope [33], which can yield low background gamma rays from DM annihilation.

- Particle colliders: Heavier DM particles could be produced up to TeV scale from SM collisions, possibly through a heavy mediator/portal particle (Figure 1.6 c,d) decaying visibly or invisibly. For invisible decays to DM particles, the experiment looks for missing transverse energy E_T^{miss}, in conjunction with an Initial State Radiation (ISR) monojet (Figure 1.7).

- Fixed target: Experiments comprising of a linear accelerator and a fixed target, or beam dump, enable particle acceleration without concern for bremsstrahlung associated with curved paths. A relevant example of this is LDMX, which closely tracks accelerated electrons impacting on a fixed target.

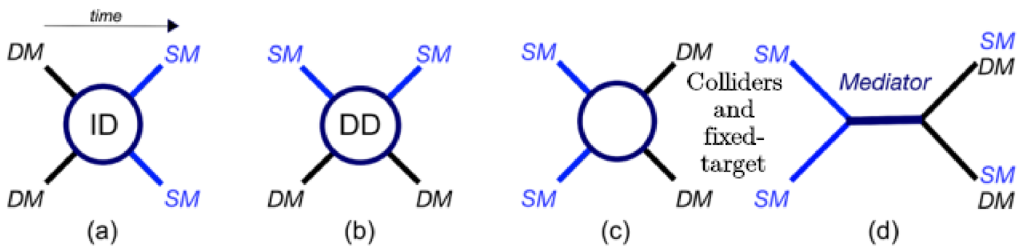

Figure 1.6: Diagrams showing the primary detection methods of DM interactions; (a) Indirect detection-Production of SM particles directly by DM annihilation, (b) Direct detection-Scattering between DM and SM particles, (c) DM production through annihilation of SM particles, (d) DM production through a resonance from SM collisions, with visible and invisible mediator decay. [34]

There are multiple potential reasons that we have not yet observed particles beyond the SM. Perhaps these particles are so heavy, and require higher centre of mass collision energy to be produced, which is clearly the remit of the energy frontier. Perhaps the difficulty lies in how feeble the interactions of the particles are, which requires the high luminosity approach of the intensity frontier. In any case, cosmic frontier experiments can validate that particles created in the lab do correspond in reality to cosmological DM. It is clear that these areas of exploration are complementary to each other.

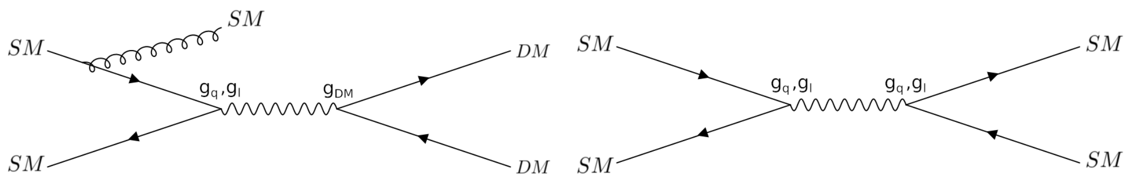

Figure 1.7: Diagrams representing the leading order processes for a vector mediator decay at a collider experiment. Invisible decays, when the mediator decays to invisible DM(left), utilise an ISR monojet in the final state. Visible decays, when the mediator decays to SM particles(right), lead to searches for dijets in the final state. Couplings are shown between mediator and SM (g_q, g_l) and between mediator and DM (g_{DM}).

Illustrating the complementarity of experimentation can be achieved by showing experiments from different frontiers on the same plots. This can highlight the exclusion potential and sensitivies of different experiments to certain Dark Matter models. Achieving a more complete picture in this way will help communication between frontiers, and assist in the future prioritization of particle physics science goals. In my case, I have focused primarily on simplified vector mediated models, specifically dark photon benchmarks, described in Section 2.4.

1.6 Community planning; Snowmass and iDMEu

To facilitate the development of experiments, and to direct public funding, decisions inevitably need to be made to prioritize some search endeavours over others. The Particle Physics Community Planning Exercise, or 'Snowmass', named after the location in which it is held, is an event held by the Division of Particles and Fields of the American Physical Society to define the most important questions in particle physics.

Originally conceived in 1982, the original mission statement was to: "Assess the future of elementary particle physics, to explore the limits of our technological capabilities, and to consider the nature of future major facilities for particle physics in the U.S."[31]. Subsequent events were held in 1984, '86, '88, '93, '96, and in 2001 with >1200 attendees. The 'Community Summer Studies' were held in 2013 and planned again for 2021 (but delayed until 2022; the year of writing). The conference has been slightly adjusted to include "international partners" but the aims remain the same.

After the analyses and discussions have been conducted, the final output of this process will be a summary book at the end of 2022, comprised of summarized reports generated from each experimental frontier. Several rounds of contributed whitepapers, by smaller sub groups from each frontier, convened with specific research goals in mind, contribute to the final output report for each frontier. This is then presented to the Particle Physics Project Prioritization Panel (P5), which takes the overall scientific input and develops the final strategic 10-year plan for U.S. particle physics, with a view to a 20-year global vision for the field overall.

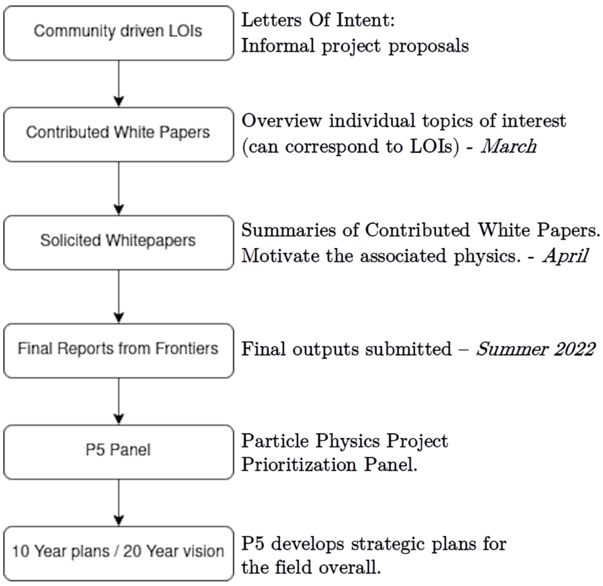

Figure 1.8: General process timeline for Snowmass 2022.

I have primarily been working within the high energy collider focused snowmass group 'EF10 - BSM: Dark Matter at colliders', which at the time of writing was co-convened by my supervisor Dr. Caterina Doglioni (Lund University), Prof. LianTao Wang (University of Chicago) and Prof. Antonio Boveia (Ohio State University). This group aimed to address the complementarity aspect of collider searches with respect to other probes. Out of a number of whitepapers in this group, the two that I have contributed to so far are related to the following letters of intent:

- LOI #21: Displaying Dark Matter constraints from colliders with varying simplified model parameters [35]
- LOI #34: Summarizing experimental sensitivities of collider experiments to Dark Matter models and comparison to other experiments [36]

Additionally of interest and relevance, there is LOI #150: Dark Matter Complementarity [37], with the goal to illustrate how future searches for WIMP and light Dark Matter are complementary across frontiers over the next decade.

An initiative relevant to this work is Physics Beyond Colliders (PBC). PBC has the stated goal of "exploratory study aimed at exploiting the full scientific potential of CERN's accelerator complex and scientific infrastructures through projects complementary to the LHC and other possible future colliders." [38]. 'Complementary to the LHC' in this context refers partially to the intensity frontier of accelerator and fixed target experiments.

Another community effort conducted in Europe, on a smaller scale and with a focus on Dark Matter specifically, is the initiative for Dark Matter in Europe and beyond (iDMEu)[39]. Their mission statement is: "Toward facilitating communication and result sharing in the Dark Matter community". As already discussed, the Dark Matter research community is diverse, and constraining these phenomena requires broad cross frontier discussions to be most effective. It is crucial to create a permanent online platform for sharing and collaboration, if we are to uncover particle evidence for Dark Matter, beyond the astrophysical observational evidence that we have.

To that end, I also began work to briefly review the current state of dark photon experiments, the focus of this work, tabulated for the iDMEU website, and included in section 4.2 of this thesis. This work will be continued as part of a future student project at Lund University.

2 Motivation

2.1 The convenient WIMP

The questions surrounding Dark Matter; where it came from, how it interacts, whether it is particulate in nature, all still require answers. Could Dark Matter interact with normal matter at all? Were they coupled somehow at some point in universal history?

Within the framework of *Thermal Relic Dark Matter* [42], the processes that produce and annihilate Dark Matter were happening at equal rates in the early universe, and the total amount of DM was unchanged (Region I in Figure 2.1). Similar to the principle of photon decoupling which occurred approximately $300,000$ years after the Big Bang and led to the Cosmic Microwave Background Radiation (CMBR), the expansion rate reached a point where Dark Matter interactions became decoupled from the rest of the universe. At a certain point, the temperature of the early universe fell below the mass of the Dark Matter, leading to production being kinematically prevented.

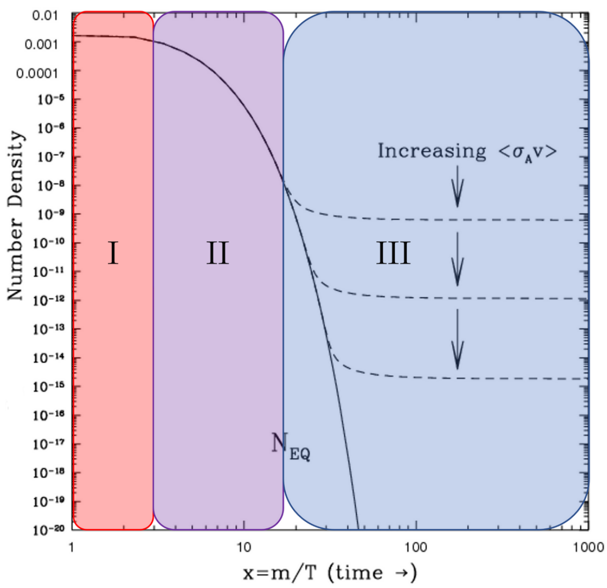

Figure 2.1: Dark matter density as a function of universal thermal expansion. The solid line is equilibrium density. Dotted lines are frozen out relic density for different energy-averaged self annihilation cross sections $<\sigma_A v>$. v is the relative velocity of a DM pair. Region I: annihilation rate = production rate. Region II: production rate ceases. Region III: annihilation ceases.[40][41]

As Dark Matter continued to annihilate with itself with a cross section σ, the corresponding rate of annihilation is given by σv where v is the relative velocity of each DM particle pair. As annihilation ocurred, the DM number density would drop (Region II in Figure 2.1).

Separation between particles would eventually prevent annihilation processes from ocurring, 'freezing out' the abundance at a constant level (Region III in Figure 2.1). This leaves what is referred to as the *relic abundance*, which is inversely proportional to the annihilation cross section since a higher cross section would lead to more Dark Matter annihilating away.

The *weak scale* usually refers to particles that are comprised of anything from a few GeV in mass to TeV mass scales, with a coupling strength similar to that of the weak interaction. The so called WIMPs (Weakly Interacting Massive Particles) are a long standing candidate for Dark Matter, due to the fact that they naturally freeze out in the range of the relic density that we observe today. This convenient fact is usually referred to as the 'WIMP miracle'. More accurately, the use of the word 'weak' in the name refers specifically to the weak coupling. This can be extended to even feebler couplings by the term *FIPS*; Feebly Interacting Particles. Below the GeV scale, Dark Matter canditates can still be considered WIMPs by definition, but are usually referred to as *Light Dark Matter*.

Calculating the relic density of theoretical models can provide a bound on the parameter space of simplified models for Dark Matter interactions. If a given model over produces Dark Matter leading to too much relic abundance, it is unlikely that the model in question is an accurate description of reality, unless other early universe mechanisms are in place. If a given model under produces DM, it could still be valid part of a deeper and more complicated description, so the limit at that point still provides a valid constraint on the model. See Section 3.3 for more detail.

2.2 Searching for darkness

More and more, we hear that WIMPs are becoming less and less likely to be the main component of Dark Matter. This is because more of the mass parameter space continues to shrink as experimental data is produced and analyzed, and certain parameter ranges are excluded. Alternative answers to the Dark Matter question are far reaching. One solution could be what is called *hot* Dark Matter, so called because its particles are extremely low mass, and relativistic as a result. An abundant particle fitting this description, as well as having the required characteristic of being weakly interacting, is the neutrino. Hot Dark Matter has become less popular due to problems arising during the structure formation of the universe. The galactic distribution across the universe now is likely due to the clumping of small density fluctuations in the early universe; fluctuations which would be prevented by the relativistic nature of neutrinos. SM neutrinos have been ruled out by simulations on the basis that galactic clustering cannot be reproduced [43], and it is generally accepted that if hot Dark Matter makes up any measurable proportion of the observed abundance, it is a low proportion.

Cold Dark Matter on the other hand, covers a wide range of possibilities, including WIMPs, primordial black holes, and axions. This theory is consistent with galactic clustering, and lends its name to the Standard Model of cosmology, knows as the 'Λ-CDM' model.

Primordial black holes, so called because these black holes theoretically formed in the very early universe, also provide an alternative explanation. However, gravitational lensing measurements from supernova observations have constrained these tightly enough to conclude that, like hot Dark Matter particles, if they do contribute to the overall Dark

Matter density, it is not by much[44].

Axions are theoretical particles which go beyond the question of Dark Matter in physics, because they were postulated to address the *strong CP problem*. This is the name given to describe the fact that QCD should, according to quantum field theory, permit the violation of charge conjugation (C) and parity (P) symmetries in its interactions. This violation has never been observed in any QCD interaction, but there are no apparent reasons why this should be the case. In 1977, Peccei and Quinn proposed that the CP violating term in the QCD Lagrangian, Θ, could be treated as a quantum field. This helped by removing the need for a fine-tuned parameter in the SM, which had been experimentally constrained to near zero, at the expense of having a new scalar particle resulting from excitations of this field. This particle is the axion. This is known as the *Peccei-Quinn mechanism*[45], and the symmetry under which the new scalar field is charged is known as the *PQ symmetry*. The axion is as yet undiscovered, but provides a strong candidate for Dark Matter.

However, due to the aforementioned 'miracle' that WIMPs reproduce the observed relic density, as well as the facts that WIMPs are predicted by other extensions to the SM such as Supersymmetry, and that the WIMP mass parameter space is in the range of our current experiments, they still remain one of the top candidates.

There are different mechanisms, or *portals*, for the SM particles to interact with the space of Dark Matter states, often referred to as the *dark sector*. It is advantageous to prioritize the simplest possible models for these mechanisms, in order to make optimal use of the parameter space that is experimentally accessible.

The thermal relic abundance provides a bound against which the parameter space for a given model can be constrained. In a simplified thermal relic model, the early universe interaction mechanisms between SM particles and DM particles are assumed to be simple. If a region of mass parameter space requires the couplings between SM particles and the DM mediator (g_q, g_l, recall Fig. 1.7 in Section 1.5) to be very large in order not to over produce according to the observed relic abundance, then perhaps those mass combinations should not be prioritized, because they point to a more complicated interaction relationship. I will present a discussion of this in Section 3.3. If the relic abundance is not met, and Dark Matter is *under produced* for certain parameters, this could be due to the richness of the dark sector in reality, and is not grounds for excluding those coupling values.

While complicated models of the dark sector can be more tightly constrained by experimental results, this is at the expense of this ease of comparison between experiments and frontiers. It is necessary to work inside a common theory framework, for example that of simplified models, and this can be utilized to compare results more easily.

2.3 Minimal models

The simplest experimental DM signal that could be expected at a collider such as the LHC, is a large amount of missing transverse energy from the DM particles escaping the detector, E_T^{miss}, recoiling against a single final state jet, known as a *monojet*. Missing momentum signals like this rely on the conservation of momentum, which in the initial state of the colliding protons was zero in the direction transverse to the beam. The non zero transverse momentum of the final state monojet therefore indicates potential Dark Matter candidates recoiling with the equal and opposite transverse momentum. Recall that the diagram for this process was presented in Section 1, Fig. 1.7.

During runs 1 and 2, the LHC's ATLAS and CMS experiments have amassed a wide range of data on these "mono-X" final states, which cover a lot of different SM particles, and which correspond to the decay of newly proposed, weakly coupled mediators. These mediators are part of a common set of simplified models recommended by the LHC Dark Matter Working Group (DMWG), formerly the Dark Matter Forum [46], to be used to compare standardized results between experiments. *Minimal* models are in between Effective Field Theories (EFTs), which are approximations without a mediator (Fig. 2.2), and a complete theory like the Minimal Supersymmetric Standard Model (MSSM), which actually proposes a WIMP in its framework. The addition of a mediator to the model adds one more dark sector particle to an EFT, and one layer of complexity.

The primary simplified models in this context contain two particles additional to the SM; the Dark Matter is a Dirac fermion, which interacts with the SM via a heavy spin-1 mediator. Five free parameters then characterize a given model: DM mass m_{DM}, mediator mass m_{med}, coupling to quarks g_q, coupling to leptons g_l, and coupling to Dark Matter g_{DM}. These parameters determine the rate of the mediator production in proton collisions, the relevant decay rates and branching ratios, and the kinematic distributions of the signals from Monte Carlo (MC) event simulations. These models aim to set limits on parameters that are most accessible by current experiments.

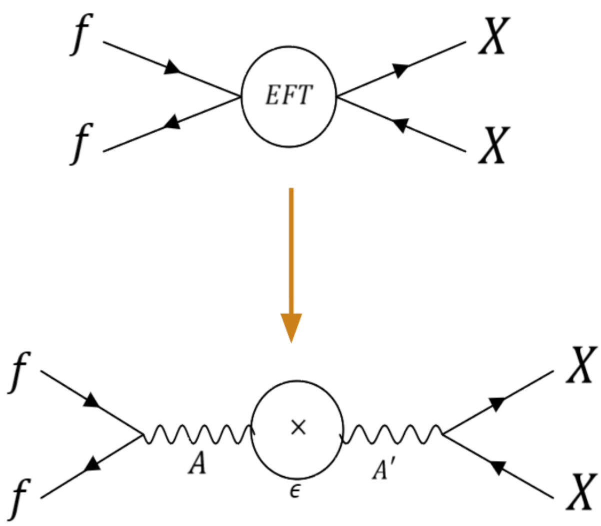

Figure 2.2: Diagram showing an EFT for a WIMP model (top) and the addition of a mediator (bottom) to make a *simplified* model. ϵ is the mixing parameter between the photon A and the dark photon A'. X could be SM (visible) or DM (invisible) decays.

The term *benchmark* refers to a framework of model parameters such as coupling and mass combinations, for which an exclusion sensitivity limit is determined for a set of generated events. The limits for a given set of couplings can then be rescaled to another set, differing only in cross section, if the cross section for the other signal is known. This requires analytical approximations for the cross sections of a certain set of couplings within a model, but leads to an ease of comparison between results from different sources, without the need for generating monte carlo events for every signal, which would become prohibitively resource heavy. It has been the remit of the DMWG to determine the optimal strategies for interpreting and reporting results from LHC, for comparison with other experiments.

As well as a spin-1 vector mediated model, other minimal benchmarks outside of the scope of this paper include an *axial-vector mediator*, also spin-1, and spin-0 mediated models where the couplings are *scalar* or *pseudoscalars*. Depending on the model, the Dark Matter itself could be a *pseudodirac* fermion or a *majorana* fermion, with spin-$\frac{1}{2}$, or it could be a spin-0 scalar or pseudoscalar. *Majorana* refers to the particle being its own antiparticle. Each of these Dark Matter types yields a slightly different thermal relic density target. This discussion will focus on Dark Matter of the psuedodirac kind, meaning that if antiparticles exist for the DM, they theoretically should have half integer spin.

Scalar and vector particles are named that way because they transform under a specific representation of the Lorentz group, which is comprised of boosts and rotations. A scalar transforms under the scalar representation, and a vector under the vector representation, and so on. *Pseudo* in this context refers to a particle or quantity's behaviour when it undergoes transformations. An example is the magnetic field vector, $\vec{B}$, which undergoes a sign change when it is reflected. It is therefore in actuality an *axial* or *pseudo* vector.

These LHC simplified models only contain couplings between the mediator and SM fermions, and mediator to DM fermions. There is a single coupling to quarks g_q and a separate coupling to leptons g_l [46]. In this discussion, the coupling to leptons g_l will be neglected. ATLAS and CMS have tightly constrained the bounds on these models from dilepton searches for any $g_l > 0$; setting the coupling to leptons to zero avoids this.

The interaction Lagrangian for a general vector mediated model coupling only to quarks is shown in Eq.2.1[47], where the mediator is denoted by Z', and the Dark Matter by χ.

$$\mathcal{L}_{\text{vector}} = -g_{DM} Z'_\mu \bar{\chi}\gamma^\mu \chi - g_q \sum_q Z'_\mu \bar{q}\gamma^\mu q \tag{2.1}$$

The gamma matrices γ^μ manifest as a result of first interpreting the standard Schrödinger equation, which describes the wave functions of non relativistic particles, but in terms of the relativistically invariant relationship between energy and spatial momentum. This leads from the free Schrödinger equation (Eq.2.2) to the *Klein-Gordon* equation (Eq.2.3), which describes relativistic scalar fields; that is, fields which transform as singlets under the Lorentz group of boosts and rotational transformations. One further step, proposed by Dirac in 1928 [48], was to try to find an equation which was linear in spatial and time derivatives, and did not require the particle to be a scalar (ϕ), so that it would also apply to fermions (ψ) with half integer spin.

$$i\frac{\partial \phi}{\partial t} = -\frac{1}{2m}\nabla^2 \phi \tag{2.2}$$

$$(\partial^\mu \partial_\mu + m^2)\phi = 0 \tag{2.3}$$

$$(i\gamma^\mu \partial_\mu - m)\psi = 0 \tag{2.4}$$

Dirac added four unknown constants into his template equation, linear in its derivatives, and noted that applying its operators twice yielded an equation of the form of the

Klein-Gordon equation. He used this to constrain his unknowns, and from this the four 4×4 *Dirac* or γ-matrices emerged, constructed from arrangements of the Pauli matrices (σ^i). The exact form depends on the basis in which the matrices are expressed. The two common bases are, first, the *mass* basis, which is appropriate to use in conjunction with fermions represented by spinors; that is, their spin state. Secondly, the *Weyl* basis, which is only slightly different, simplifies the expression of the fermions in their chiral basis. That is, when distinguishing the left chiral and right chiral projections of the fermion states. The weak interaction couples only to left-chiral states, so nature actually distinguishes matter in the Weyl basis.

The Lagrangian density term in Eq. 2.1 for the vector mediated coupling to the quark states will yield the appropriate equation of motion corresponding to the wave equation expressed by Dirac in Eq.2.4. The γ matrices are expressed below, first in the mass basis (Eq. 2.5), and then in the Weyl basis (Eq. 2.6).

$$\gamma^0 = \begin{bmatrix} 1 & 0 \\ 0 & -1 \end{bmatrix}, \quad \gamma^i \begin{bmatrix} 0 & \sigma^i \\ -\sigma^i & 0 \end{bmatrix} \tag{2.5}$$

$$\gamma^0 = \begin{bmatrix} 0 & 1 \\ 1 & 0 \end{bmatrix}, \quad \gamma^i \begin{bmatrix} 0 & -\sigma^i \\ \sigma^i & 0 \end{bmatrix} \tag{2.6}$$

The decays of the mediator are therefore shared between decays to Dark Matter χ and decays to quarks. Eqs. 2.7 and 2.8[47] give the expressions for the mediator's partial widths. Patial widths are proportional to the branching ratios; the number of decays which happen by a particular decay mode, as a fraction of the total decays. The Δz's refer to the mass ratio for each particle compared to the mediator; either $\frac{m_{DM}^2}{m_{med}^2}$ or $\frac{m_q^2}{m_{med}^2}$. For these decays to be kinematically possible, the mass of the decay products, quarks or Dark Matter, are constrained by the conservation of energy such that $m_{med} \geq 2m_{DM,q}$.

$$\Gamma_{vector}^{\chi\bar{\chi}} = \frac{g_{DM}^2 m_{med}}{12\pi}(1 - 4\Delta z_{DM})^{\frac{1}{2}}(1 + 2\Delta z_{DM}) \tag{2.7}$$

$$\Gamma_{vector}^{q\bar{q}} = \frac{g_q^2 m_{med}}{4\pi}(1 - 4\Delta z_q)^{\frac{1}{2}}(1 + 2\Delta z_q) \tag{2.8}$$

2.4 The dark photon

In a basic vector mediated model, the couplings to the SM are free parameters. In a specific version of a vector mediated model, the mediator is known as the *dark photon*. In this case, the coupling to the SM manifests as a result of mixing between gauge groups, leading to an interaction term in the Lagrangian. Since the dark photon in this case mixes in a well defined way with particles from the SM, such as the SM photon or the Z-boson, the couplings to the SM are fixed. This is what differentiates the dark photon from a more general vector mediator. The most common ways to refer to a dark photon are as either A', Z_D or Z'.

The current SM is described by the framework of QFT, in which it is fully represented by a Lagrangian. The gauge groups refer to transformation sets which leave the

Lagrangian, and hence the kinematic behaviour of the model, invariant. The three distinct gauge groups whose transformations leave the SM Lagrangian invariant, are:

$$SU(3) \times SU(2) \times U(1) \tag{2.9}$$

This product is a *direct product*, which in group theory means that the generators of the groups do not mix. For example, the generators of the $SU(3)$ operations, corresponding to the gluon octet, do not mix with the weak hypercharge and weak isospin generators of the unified $SU(2) \times U(1)$ group. Consider for example a quark, which is a color charged particle corresponding to a triplet state under $SU(3)$ transformations. This means that they can oscillate between different distinct color states; red, green and blue, depending on their transformation by the emission or absorption of a gluon, the mediator of the color force. All other fields in the SM however, like the leptons and other bosons for example, are singlets under $SU(3)$. This amounts to the same thing as saying that they are not colour charged; they are not charged under $SU(3)$.

Above a certain energy, known as the electroweak scale energy, the latter two gauge groups $SU(2) \times U(1)$ are united into a single symmetry known as *electroweak symmetry*. The generators of this single symmetry group require four massless bosons, W_1, W_2, W_3, B. Since, in nature, we observe 3 massive bosons, the W^+, W^-, Z^0, and one massless photon, associated with the separated weak and electromagnetic fields, something additional is required to happen at the electroweak energy scale. This 'something' is the *Higgs mechanism*, which is responsible for spontaneous symmetry breaking between these two fields, known as *electroweak symmetry breaking*. This process leads the W_1, W_2 bosons to acquire mass, and become the W^+, W^- bosons. It also leads to the W_3, B particles to be rotated, by the weak mixing angle θ_W, into becoming the states of the massive Z^0, and the massless photon γ. The photon of electromagnetism remains massless because it, along with its associated unbroken $U(1)$ symmetry, does not couple to the Higgs field, and does not acquire any mass.

The dark photon has its name because it is analogous to the SM photon; it is the gauge boson of a proposed new unitary gauge field, which is included instead of the regular SM electromagnetic $U(1)$ symmetry; $U(1) \rightarrow U(1)_a$ and $U(1)_b$. This gauge field has been spontaneously broken by an interaction with a similar *dark* Higgs field, known as the *Hidden Abelian Higgs Mechanism*[49], and it couples directly to the Dark Matter particle. This fixes the SM couplings due to the mixing, and reduces the number of unknown parameters to four; M_{DM}, M_{med}, g_{DM}, and mixing parameter ϵ which describes to what extent the new coupling is suppressed with respect to the electromagnetic coupling. The mixing parameter ϵ is related to a θ_W-equivalent *dark mixing angle* θ_a by $\epsilon = \sin\theta_a$, hence the name *mixing parameter*.

The smaller the number of parameters in a theory about new physics, the more effectively it could highlight new discoveries. Experimental discrepancies with the SM should be more visible when observed in terms of a model with only a few unknown parameters, and thus a smaller parameter space. The caveat is of course: nature may not be so kind as to provide us, in reality, with a model containing few parameters.

$$\mathcal{L} = -\frac{1}{4}F_{\mu\nu}F^{\mu\nu} \rightarrow -\frac{1}{4}F_{a\mu\nu}F_a^{\mu\nu} - \frac{1}{4}F_{b\mu\nu}F_b^{\mu\nu} - \frac{\epsilon}{4}F_{a\mu\nu}F_b^{\mu\nu} \tag{2.10}$$

$$\mathcal{L} = eJ_\mu A^\mu \rightarrow \mathcal{L}' = \Big[\frac{e'}{\sqrt{1-\epsilon^2}}J'_\mu - \frac{e\epsilon}{\sqrt{1-\epsilon^2}}J_\mu\Big]A'^\mu + eJ_\mu A^\mu \tag{2.11}$$

The standard kinetic term in the SM Lagrangian for the photon field, is expanded to include an additional term corresponding to the second $U(1)$ group (Eq.2.10)[50], and a mixed kinetic term containing the field strength tensors for both photon fields. These two new fields A_b, A_a are then rotated to diagonalize this kinetic term; they are rotated to remove the mixed term so that it resembles a free field theory of two separate photon fields, which yields the change to the interaction term shown in Equation 2.11[50]. A and A' correspond to the SM photon, and the dark photon respectively. In this case, the dark photon is considered to be massive, which forces the direct coupling of A' to the SM current in Eq. 2.11, allowing for the possibility of detectable signatures experimentally. The Feynman diagram shown earlier, in Fig. 2.2, corresponds to the mixing between these two photon states.

$$\mathcal{L}'_D = \Big[\frac{e'}{\sqrt{1-\epsilon^2}}J'_\mu - \frac{e\epsilon}{\sqrt{1-\epsilon^2}}J_\mu\Big]A'^\mu \tag{2.12}$$

$$\implies \mathcal{L}'_D \rightarrow \mathcal{L}''_D = \Big[\frac{e'}{\sqrt{1-\epsilon^2}}J'_\mu - \frac{e\epsilon}{\sqrt{1-\epsilon^2}}J_\mu \quad \boxed{-\frac{e'\epsilon_Z}{2\cos\theta_W}J_\mu^{NC}}\quad\Big]A'^\mu$$

Consider now that the extended $U(1)_D$ gauge field instead mixes kinetically with the unitary weak hypercharge group $U(1)_Y$ from before the electroweak symmetry was broken by the Higgs. This leads to a more general dark photon model in which A' also couples to the Neutral Current (NC) of the Z boson in the SM. This is shown in Eq. 2.12[50][51][52], where ϵ_Z is a mixing parameter with the Z boson, which is treated separately to the photon mixing. Since the weak mixing angle θ_W determines the Z boson and photon states from the W_3 and B states at the point of electroweak symmetry breaking, it also factors into this coupling with the dark photon.

In a dark photon model such as this, the couplings to the SM are restricted by the fixed couplings within the SM itself. The fixed couplings between the Z and the quarks and leptons of the SM indicate that the dark photon couplings are also fixed.

2.5 Model simulation and jets

To make comparisons between models, and determine how results can possibly be translated between them, it is necessary to generate events using Monte Carlo (MC) simulation methods, in order to examine how the signals are distributed in different cases.

The MC event generating package used in this work was MadGraph5 (MG5) [53], which is a general package containing the ability to simulate data for a variety of BSM models. MG5 generates stochastic collision events between partons, in this case for proton collisions like those at the LHC, after taking the Lagrangian of a given model as an input. The Lagrangian determines the applicable Feynman diagrams, and associated matrix elements which determine the scattering amplitudes, for each process. MG5 can interface with Pythia8 [54], via a package called MadAnalysis5 (MA5) [55], to create showers at the parton level, and then hadronize them into jets. Detector simulation is then conducted using, for example, a package such as DELPHES [56], which *smears* the event at hadron level to some extent to simulate the detector effects, after which the event can be reconstructed. MG5 is capable of outputting plots of different kinds depending on how it is steered; its output format (.hepmc files) can also be passed to an analysis package, such as RIVET [57], for a wide range of analysis requirements. These .hepmc files are *event files*, which list all the details of simulated collision events, and are of a standard format in the world of high energy physics, for MC event generator outputs.

RIVET is a toolkit aimed at the preservation of all analysis code associated with collider physics. It is comprised of a growing set of experimental analyses, and it implements a faster 'smearing and efficiency' approach distinct from that of DELPHES, used by Madanalysis, which models detector geometry and particle-material interactions [57].

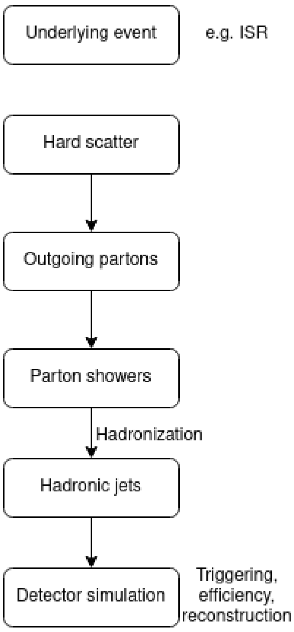

Figure 2.3: Basic flow diagram of simulation procedure, from inital scatter to detector simulation.

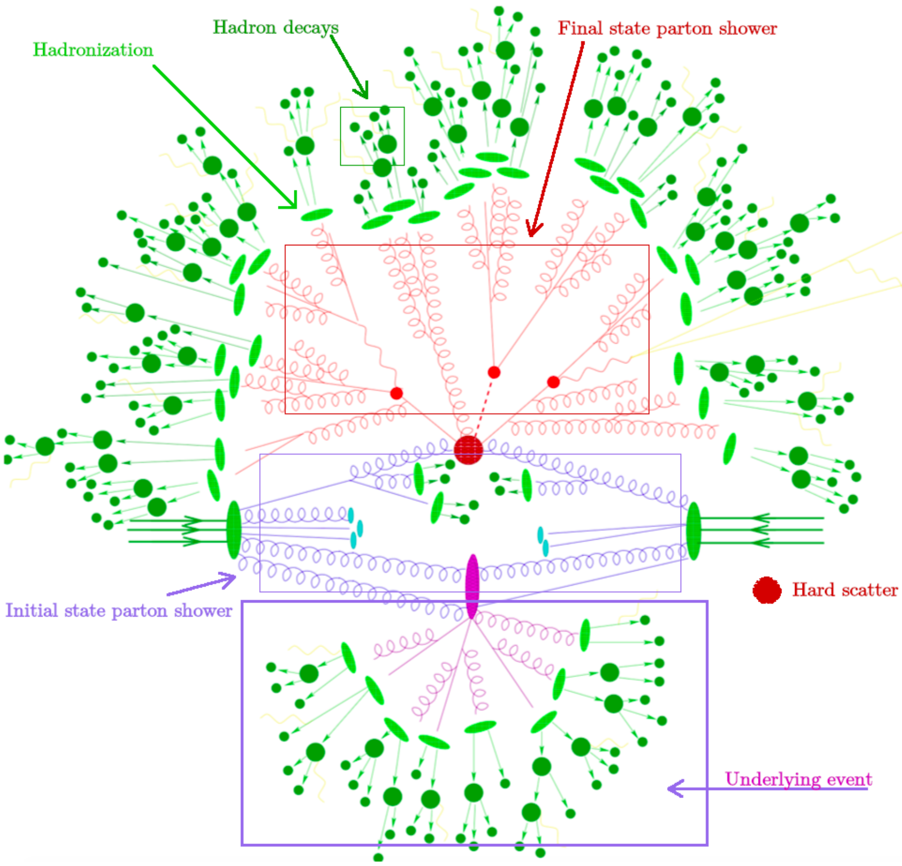

Figure 2.4: General schematic representation of Monte Carlo event generators for proton proton collisions, highlighting the hard scatter of partons, and the subsequent hadronization. Original image from Sherpa MC event generator [58].

The general progression is shown in Fig.2.3, which encapsulates on a very basic level all that is seen in a hadron collision. The *underlying event* refers to everything 'else'; that is, all that is not coming from the primary hard scatter between partons. This can include initial state radiation, which itself can hadronize into a jet detected in the experimental setups.

Jets are groups of particles which are associated experimentally with a common starting point, called a *vertex*, and are correlated within a roughly conical shape. Ideally, particles in a jet can be idetified and grouped together so that they can be associated with a single vertex from which their production began. This definition of a jet is applied at different levels of the scatter: parton level, and particle level, which refer to before and after hadronization. This is clarified in Fig.2.4 which attempts to illustrate the stages of a proton collision, from parton hard scatter, to hadron jet detection.

The hard scatter is represented by the red central vertex. Running into this are two of the partons from the beam protons, which are themselves represented by green ovals on the left and right. The scattering is governed by QCD, and since gluons are self interacting, they can emit additional gluons as well as creating $q\bar{q}$ pairs, which leads to *parton showers*, shown in red.

As the energy scale falls, *hadronization* ocurrs when it becomes energetically favourable for the vacuum between high energy color charged particles, such as quarks and gluons, to pair produce more quarks due to QCD confinement. Since gluons are self interacting, as the separation between two high energy quarks grows, the energy density also grows, confining the field between them. The *Lund String Model* [59] (Fig.2.5[60]) illustrates how hadronization between two separating high energy quarks can confine the showering partons into colourless hadrons, grouped together in jets. The yellow lines represent non vanishing fields between the quark pairs, and the conical shape of the jet is evident between the two highest energy quarks on the far left and right.

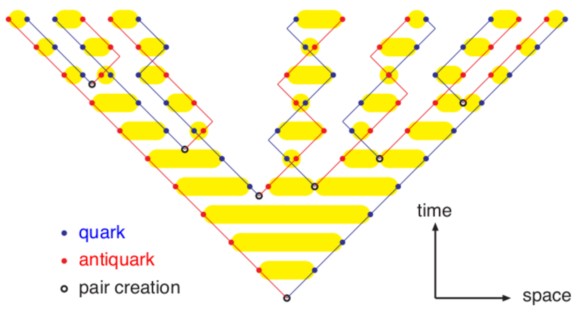

Figure 2.5: Strings representing a separating $q\bar{q}$ pair, illustrate how field energy causes on shell pair production of additional $q\bar{q}$ pairs in between.

To connect this back to the signal with which we are most interested in the context of vector mediated Dirac Dark Matter models, consider again the diagram shown earlier in Section 1 in Fig.1.7, illustrating the leading order final state consisting of a single jet from an ISR gluon, if the mediator decays invisibly. In the process of interest, this high energy gluon will pair produce quarks which will hadronize in the manner described above. The calorimeters will measure the energy of the resulting high P_T jet of hadronic decay constituents, which will indicate a missing P_T of equal magnitude and opposite direction, corresponding to the invisible Dark Matter particles.

An event display for such a monojet event, is shown in Figure 2.6. The energy deposits in the calorimeter layers are visible, and the angular distribution of the detected energy deposition is shown on the right, forming one distinct peak.

Exclusions from monojet or invisible final states are kinematically constrained by the fact that $m_{med} \geq 2m_{DM}$ in order for the mediator to decay to invisible final states.

This can be seen in Appendix A in Fig. 5.3 by the relegation of the associated monojet exclusion regions to below the $m_{med} = 2m_{DM}$ line. The dijet final states, shown back in Section 1.5 in Fig. 1.7, are not constrained by the kinematics in this way, as also reflected in the mass-mass plot in Fig. 5.3. In that case, the kinematic constraint would come instead from the quark masses.

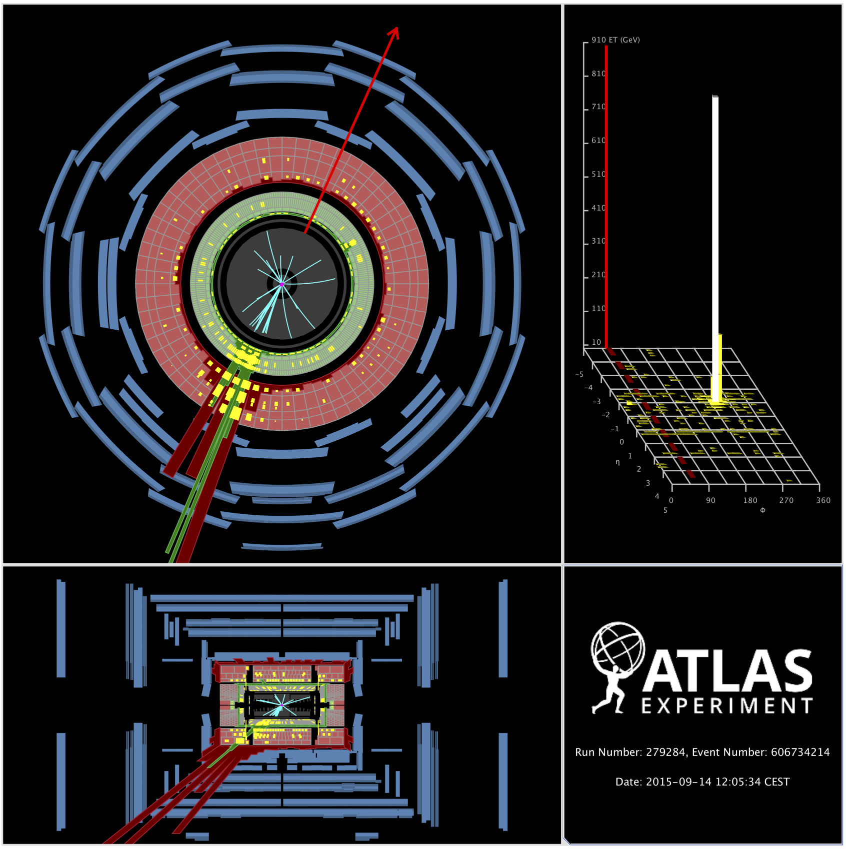

Figure 2.6: The highest E_T^{miss} monojet event in the 2015 ATLAS data. A jet with $p_T = 973$ GeV, indicated by the green and red bars corresponding to the energy deposition in the calorimeters, is balanced by a E_T^{miss} shown as the red arrow. [61].

A three jet final state is also feasible, which is a combination of the mono and dijet signatures. An ISR jet could also be produced alongside a visible mediator decay mode, much like in the case of the best evidence available for the existence of gluons. In that case, since quarks are pair produced, a third radiated particle, the gluon, is required to explain the third jet in such observations such as those made by the TASSO collaboration at PETRA in 1979 [62].

In summary, experiments across different frontiers can be sensitive to different final states, for example invisible or visible decays of a Dark Matter mediator. Tools from multiple frontiers are required to complement each other in the constraining of model parameters.

3 Analysis

The overall goal is to translate, or *scale*, current constraints on a vector mediated DM model, obtained from monojet data at the LHC, to constraints on a dark photon model. The LHC data spans the mediator mass range of 100 GeV to approximately 2 TeV. The constraints are in the form of an upper limit on cross section; if the cross section of a process is less than this limit, then the experiment is not sensitive enough to constrain it. This can be referred to as a *sensitivity limit*.

The approach is to first reproduce the LHC limits with MC simulated events, using a vector mediated model at leading order in MadGraph, and to obtain the expected sensitivity to signal events using CMS data collected over the previous LHC run. This value has the units of cross section, in *pb*, and can theoretically be *scaled* to an equivalent cross section limit for a different set of initial parameters, or for a different model such as a dark photon model. The CMS limits are first extended to the *low mass* range, down to 10 GeV mediator mass, within the same vector mediated model. In order for the limit to be scaled to a different model, the detector simulation acceptance must be equivalent, so that the distribution of the missing energy does not differ in shape.

I have first demonstrated that, within the vector mediated model, altering the Dark Matter type from Dirac DM to complex scalar DM does not change the shape of the distribution. Following that, I demonstrate that changing between the vector and dark photon mediated models in question, also does not alter the distribution shape, indicating that the cross section sensitivity limits can be scaled between models. Other experiments may require, for example, a DM type other than complex scalar DM within the vector mediated model, and would then also require a similar analysis. I have included Dirac DM to complex scalar just as an example.

3.1 Acceptance testing

The first MG5 model that I began simulating with is the FeynRules[63] simplified Dark Matter model 'DMSimp'[64], which includes multiple types of Dark Matter and mediator particles. The Lagrangian for DMSimp contains spin-0 scalar and spin-1 vector mediators for scalar and Dirac type Dark Matter. There are separate coupling parameters for each mediator to each type of Dark Matter, and each mediator to each quark and lepton individually. This means that the mediator can couple independently to individual quarks and leptons, with coupling strengths that are not fixed. This is not strictly a dark photon model, but rather a more general vector mediated model. There is complete freedom to choose how the model behaves in terms of couplings, and the masses of each particle can be individually set.

The quantities of interest for the analysis are firstly the missing total transverse energy, (which is the detected sum of transverse momenta in the simulation), and secondly the transverse momentum P_T of the leading jet (jet 1). Figures 3.1 and 3.2 show examples of these analyses, applied to hepmc files generated by MG5. The process generated is a proton-proton collision at LHC centre of mass energy, where the mediator that is produced decays invisibly to Dark Matter. A monojet appears in the final state from ISR, which is analyzed and plotted in RIVET. The corresponding Feynman diagram is shown earlier in Fig. 1.7.

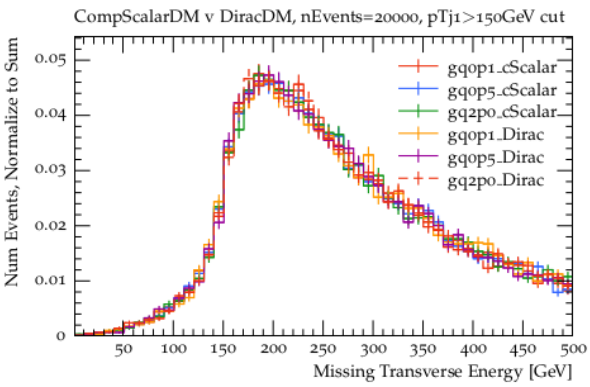

Figure 3.1: E_T^{miss} distribution comparison for DMSimp model between complex scalar and Dirac Dark Matter types, for three different quark couplings; $g_q = 0.1, 0.5, 2.0$. $m_{med} = 2250$GeV. Process is $[p\,p\, >\, x\,\bar{x}\,j]$ at $\sqrt{s} = 13$GeV, # events = 20000, and a minimum transverse momentum cut on leading jet of $P_T > 150$GeV. Each curve is normalized to facilitate shape comparison.

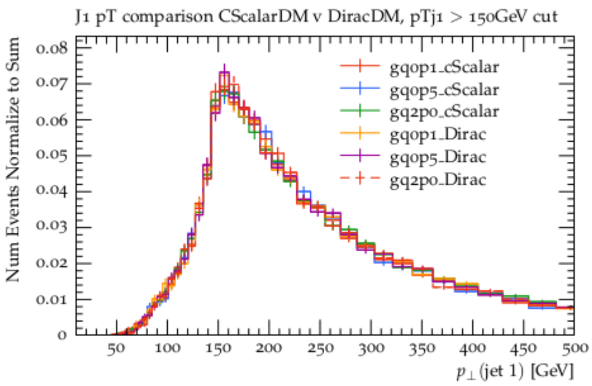

Figure 3.2: Leading jet transverse momentum distribution comparison for DMSimp model between complex scalar and Dirac Dark Matter types, for three different quark couplings. $m_{med} = 2250$GeV. Process is $[p\,p\, >\, x\,\bar{x}\,j]$ at $\sqrt{s} = 13$GeV, # events = 20000, and a minimum transverse momentum cut on leading jet of $P_T > 150$GeV. Normalized to facilitate shape comparison.

Acceptances are part of the detector data acquisition process at the LHC, in order to throw away events which are certainly part of SM background. A calculated sensitivity limit cannot be rescaled to signal parameters with very different acceptances, so the aim of this comparison was first to analyze the differences between the acceptances within the same model, comparing two Dark Matter types with the same selections applied. The only things varied in each configuration are the Dark Matter type, and the quark couplings. The curves have been normalized to their sum, meaning that the relative number of events between curves has been divided out, in order to facilitate the comparison of the shapes of the distributions. As may be expected[46], the quark coupling does not change the shape, only the number of events (which is not shown due to normalization). However, the shape is also unchanged between Dirac and complex scalar Dark Matter types, which indicates that the only thing varying between DM types is the cross section.

This illustrates that Dirac DM limits can be reinterpreted as scalar DM limits by scaling only the cross section, which means there is no need to produce separate MC simulations for different Dark Matter types in this model. This saves on time because fewer MC events need to be generated and processed. These checks on detector acceptances have been presented to illustrate the importance that only the cross section varies, in order to scale limits between models with different parameters.

Each of these RIVET generated histograms were validated against outputs from MadAnalysis to ensure they were the same. Now we have established that limits can be scaled for different DM types within this vector mediated model, the question arises of how to scale to dark photon limits, in a separate dark photon model.

The model used to investigate dark photon limits was the Hidden Abelian Higgs Mechanism model (HAHM) [49][65] (See section 2). Recall that this mechanism involves the spontaneous symmetry breaking by a dark Higgs boson of the newly introduced U(1) gauge field, where the dark Higgs can mix with the SM Higgs, changing the kinematics with respect to the vector mediated model above (DMSimp). The coupling of the dark Higgs to the Standard Model Higgs, and therefore to the SM itself, has been set to zero, in order to isolate the effect of the Z mixing, and to make the comparison directly between the dark photon and the vector mediated models.

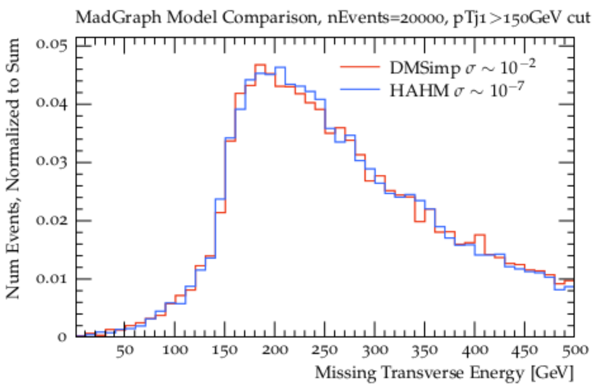

Figure 3.3: E_T^{miss} distribution example comparison between DMSimp and HAHM models. $m_{med} = 2250$GeV. $g_q = \epsilon = 0.01$. Monojet process $[p\,p\, > \, x\, \bar{x}\, j]$ at $\sqrt{s} = 13$GeV, # events = 20000, and a minimum transverse momentum cut on leading jet of $P_T > 150$GeV. Each curve is normalized to facilitate shape comparison.

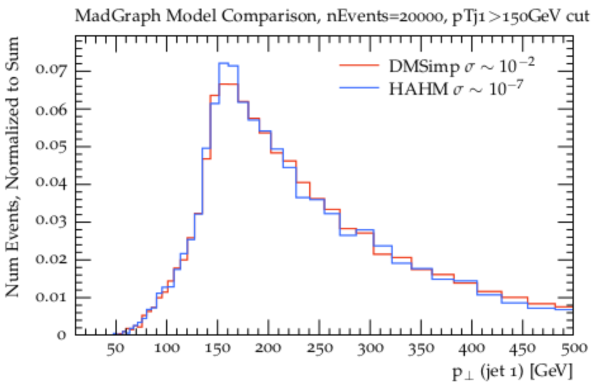

Figure 3.4: Leading jet transverse momentum distribution example comparison between DMSimp and HAHM models. $m_{med} = 2250$GeV. $g_q = \epsilon = 0.01$. Monojet process $[p\,p\, > \, x\, \bar{x}\, j]$ at $\sqrt{s} = 13$GeV, # events = 20000, and a minimum transverse momentum cut on leading jet of $P_T > 150$GeV. Normalized to facilitate shape comparison.

Figures 3.3 and 3.4 show again that the distributions for both total missing transverse energy, and the transverse momentum of the leading jet in the monojet final state for invisible mediator decay, are the same shape, and the only thing differing between the models is the cross section. The coupling to the Standard Model, whether it is quark coupling g_q or Z' mixing parameter ϵ, must be small, i.e. of the order 10^{-2}. This guarantees that the Breit-Wigner distribution of the cross section with respect to mediator mass is very narrow, and the mediator is produced on shell only. This means that the cross section approximately scales with either g_q or ϵ in an equivalent way. If the coupling becomes too large then the offshell contribution to the cross section begins to dominate, and the approximation described in the next section in Equation 3.3 breaks down.

This analysis indicates that, since the acceptances are the same when the same cuts are applied to the same process, results from CMS data can be used in MadAnalysis to calculate the low mass sensitivity limits, down to a mediator mass of 10 GeV, for both models (See section 3.2). If the acceptances were different, limit scaling between models would be less precise, and would need to involve some approximating scale factor to account for the acceptance difference.

It is also worth stating that the kinematics depend heavily on the mass of the mediator, and so scaling limits between different masses is not possible in this way [35].

3.2 Scaling limits

3.2.1 CMS upper limits

Figure 3.5 displays CMS collaboration data from searches for new phenomena in energetic monojet events with large missing transverse momentum [28].

The upper limit represents the degree to which the coupling g_q can be constrained for a vector mediated model, based on the data from CMS. It is a sensitivity limit, meaning that if the coupling strength of the dark vector mediator to SM quarks is less than this limit, then the experiment is not sensitive enough to exclude the model.

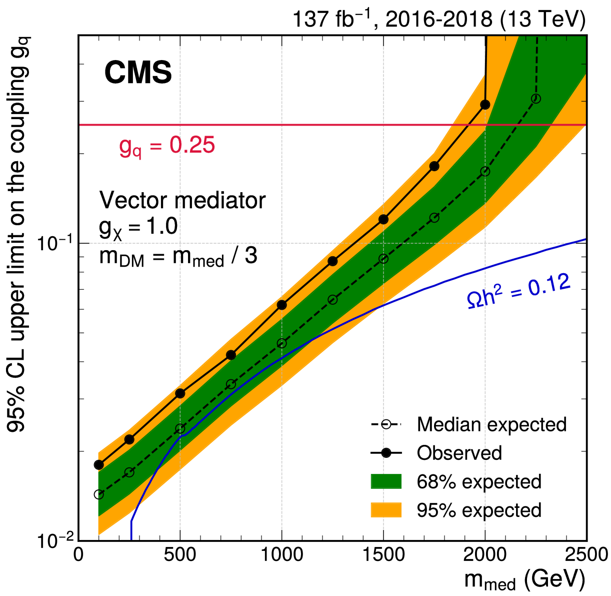

Figure 3.5: Exclusion limits at 95% CL on the couplings g_q for a vector mediator, from CMS data between 2016 and 2018. The blue solid line indicates the parameter combinations for which the simplified model reproduces the observed DM relic density. [28]

Often in the display of experimental results for Dark Matter, the relic density provides another bound with which to compare these projected sensitivities. For example, the parameter space below the relic line in Fig. 3.5 is excluded, because those parameters lead to an overproduction of Dark Matter according to a specific model. Therefore the relic line is essentially a lower bound on coupling. If this upper limit crosses the relic line, this essentially means that the associated mass range can be excluded for that model, because in that case Dark Matter must be overproduced. Beyond this relic bound, the DM could have an annihilation cross section to more hidden sector states, but in general when analyzing simplified models, such mechanisms are neglected because they are not accessible to LHC energies [66]. Above the relic line, the Dark Matter is underproduced according to the thermal relic, but this could be due to contribution from other types of Dark Matter in the hidden sector, and so the corresponding parameter space remains in play.

A commonly used plane for displaying experimental constraints on the dark photon model is that of the *yield variable* $y = \epsilon^2 \alpha_D (m_{DM}/m_{med})^4$, because the relic density roughly scales with this quantity [67]. The benchmark values that have been used here were to set $m_{DM}/m_{med} = \frac{1}{3}$ and $\alpha_D = 0.1$, which corresponds to g_{DM} by $\alpha_D = \frac{g_{DM}^2}{4\pi}$; α_D is the *coupling constant*, analogous to the *fine structure constant* α in electromagnetism, and $g_{DM} \approx 1$ in this case. With the mass of the decay products being one third of the mediator mass, this guarantees the kinematic possibility of on shell production, which is possible when $m_{med} \geq 2m_{DM}$.

3.2.2 Extending CMS limit search

This CMS limit search is re-cast in terms of the DMSimp and HAHM models, meaning the y-axis is transformed to display the yield variable, and both models can be plotted on the same axis. The results of the CMS search are extended to lower mediator masses, down to 10 GeV, using MadAnalysis5 and DELPHES for fast detector simulation.

The dark photon model, containing the Z mixing parameter, has had its constraints scaled appropriately and plotted on the yield variable plane in Figure 3.6. The vector mediated model, DMSimp, which contains the quark couplings directly, has had its constraints transformed from $g_q \to \epsilon$, and mapped onto the yield variable plane alongside the dark photon and the associated relic line. This is achieved by using the fact that the dark mixing angle θ_a can be approximately expressed in terms of the weak mixing angle θ_w, and the ratio of the masses $\Delta_z = \frac{m_{med}}{m_Z}$, as shown in [49], which gives the relationship between g_q and ϵ as:

$$\epsilon = g_q \frac{2(\Delta_z - 1)}{e \cos\theta_w} \quad \text{from} \quad g_q = \frac{e \sin\theta_a}{2\tan\theta_w} \quad \text{where} \quad \sin\theta_a \approx \epsilon \frac{\sin\theta_w}{\Delta_z - 1} \tag{3.1}$$

The way the limits are produced is as follows: MadGraph produces the MC event simulation, using leading order processes, for the overall collision event resulting in a monojet in the final state. As an example, generating this process for DMSimp in MadGraph 5 produces "21 processes with 42 diagrams", which amount to all of the appropriate leading order processes required to simulate the events. Pythia8 then takes this output and hadronises the partons before MadAnalysis uses DELPHES for the detector simulation. MadAnalysis presents an *expected* cross section sensitivity limit, calculated from the monojet analysis dataset at CMS called (cms_exo_20_004), in units of picobarns. The expected value is the theoretically expected number of events seen on top of the SM background for this model, converted to an expected cross section sensitivity.

This cross section limit is then divided by the total *reference* cross section for each process. These reference cross sections are individually generated in MadGraph, one for each specific mass and coupling parameter combination for each data point. The

MadAnalysis cross section sensitivity is now expressed with respect to the specific process cross section, and can be scaled to a limit in coupling by the cross section's relationship to g_q or ϵ. This calculated sensitivity bound ratio is proportional to ϵ^2 or g_q^2 depending on the model (see next section), so the square root of this value can be scaled to a limit in ϵ or g_q by multiplying by $\epsilon = 0.01$ or $g_q = 0.01$, again depending on the model. This is how the limit values were calculated for Figure 3.6, before being scaled to the yield variable plane shown on the plot.

3.2.3 Leading order analysis k-factor

The CMS analysis considered here is a full Next to Leading Order (NLO) analysis. NLO refers to the level of corrective terms included at the MC generator level. In an NLO analysis, higher order Feynman diagram processes are included which increases the cross section of the process overall, in comparison to a Leading Order (LO) analysis, in which only the leading order processes are considered. Often, a correction factor known as a *k-factor* is employed to account for the difference between NLO and LO cross sections.

For the CMS analysis, DMSimp was generated at NLO. Due to constraints on time, I opted to generate these MC events at LO only, and to employ a corrective k-factor to my DMSimp analysis, in order to compare my analysis directly to the CMS analysis.

For a vector mediated model such as DMSimp, the k-factor has been established to be an approximate 30% increase in cross section. This introduces a factor of $\frac{1}{\sqrt{\text{k-factor}}}$ to the sensitivity bound ratio described above, since the reference cross section has been scaled up by that factor. This then corresponds to the ability to probe a smaller coupling by a factor of $\frac{1}{\sqrt{1.3}}$.

The analysis for both the vector and dark photon mediated models have been conducted only at LO in this case. To that end, the k-factor of 30% has been applied to the DMSimp vector mediated analysis, to facilitate a direct comparison with the CMS NLO limits. The HAHM dark photon model shown on Figure 3.6 remains at LO only, because the appropriate k-factor was not known.

3.2.4 Cross section scaling

The cross section for a resonant process is a probability distribution as a function of energy, centered around the mass of the mediator particle, called a Breit-Wigner distribution. The probability is highest at the mass of the mediator, as this corresponds to the resonance being produced on-shell. Expressing this distribution as simply as possible, assuming on-shell resonance, leads to a proportionality expression for the cross section:

$$\sigma \propto \frac{g_{DM}^2 \epsilon^2}{m_{med}^4 \Gamma_{tot}} \tag{3.2}$$

Recalling from Eq. 2.7 that the Dark Matter partial width $\Gamma_{DM} \propto g_{DM}^2(1-\epsilon^2)$, then at small ϵ values $\Gamma_{tot} \approx \Gamma_{DM} \approx g_{DM}^2$. This means that g_{DM}^2 drops out of Eq. 3.2, leading to the approximate aforementioned scaling of the coupling sensitivity by $\sqrt{\text{k-factor}}$, due to:

$$\sigma \propto \epsilon^2 \propto g_q^2 \tag{3.3}$$

If the coupling becomes too large, i.e. far above $\sim 10^{-2}$, the narrow Breit-Wigner width approximation is no longer true, and the mediator's off shell contribution to the cross section becomes significant; the approximate relationship in Eq. 3.2 no longer holds, and the limits are no longer scalable.

3.2.5 Vector vs dark photon limit plot

The reason that the limit setting sensitivity shown in Figure 3.6 varies by model is because σ, and therefore ϵ^2, depends on the branching ratios inherent in the model. For a given final state, these branching fractions lead to different cross sections, and therefore a difference in ϵ^2 sensitivity between models.

As is evident, the dark photon model deviates from the vector mediated model only around the Z boson mass. This point is represented by $\frac{1}{3}m_Z$ on the x-axis of this plot, since it is the mediator at $m_{med} = 3m_{DM}$ which mixes with the Z, and contributes to the enhanced sensitivity. As m_{med} approaches the Z mass, the Z can be increasingly easily produced as it moves from off-shell to on-shell at the centre of its Breit-Wigner distribution. This is also evident in the relic density constraint line in the same fashion.

3.2.6 High-luminosity LHC forecast

A final addition to the plot are the forecast limits for the High Luminosity LHC upgrade (HL-LHC) in the context of both models. This calculation was achieved by scaling the cross section limit by the increased luminosity of HL-LHC, which scales by the square root of the integrated luminosity. This upgrade aims to provide an integrated luminosity of $3000 fb^{-1}$ [68] in total data collected, in comparison with the $137 fb^{-1}$ of data used by CMS in this search [28]. This amounts to a scaling factor of approximately 4.63.

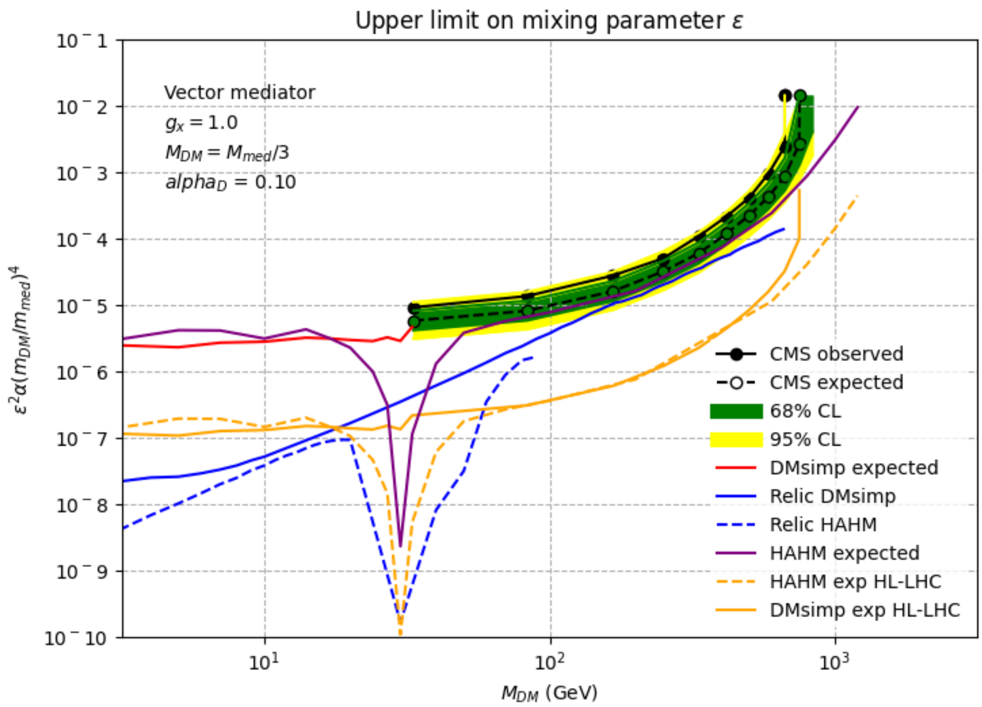

Figure 3.6: Comparison of two models, *DMsimp* and *HAHM*, corresponding to simplified vector mediated and dark photon mediated models respectively. The mass ratio between mediator and DM mass is fixed to $\frac{1}{3}$, allowing the mediator to decay to DM. The conventional dark coupling constant $\alpha_D = \frac{g_{DM}^2}{4\pi}$, with coupling $g_{DM} = 1.0$. The models have been generated with quark couplings $g_q = 0.01$ for DMSimp and mixing $\epsilon = 0.01$ for HAHM; low coupling values ensure the cross section scaling relationship with coupling by forcing the mediator resonance to be on shell. Expected and observed limits at 95% CL are plotted using the data from the CMS analysis [cms_exo_20_004] [28] for the monojet final state, at 13 TeV using 137 fb^{-1} of data. The blue relic lines represent the minimum parameter combinations which reproduce the observed thermal relic density for each model, with the expected deviation for the dark photon model around the Z resonance. Orange lines forecast the increased sensitivity of this search for these two models at the HL-LHC, estimated by the effect on the cross section of scaling up the integrated luminosity [36].

3.2.7 Intensity frontier comparison

An illuminating plot from a report on LDMX [69] (Fig. 3.7), shows the sub GeV parameter space for light Dark Matter, again in the plane of the yield variable. According to the European Strategy Briefing Book [70], and illustrated by this plot, intensity frontier experiments such as LDMX are crucial to the comprehensive search in the < 10GeV mass range as compared to the collider experiments of the energy frontier. The best sensitivity for LDMX and other intensity frontier experiments is in this mass range, and the two plots in Figures 3.6 and 3.7 display how these experiments can search complementary mass ranges.

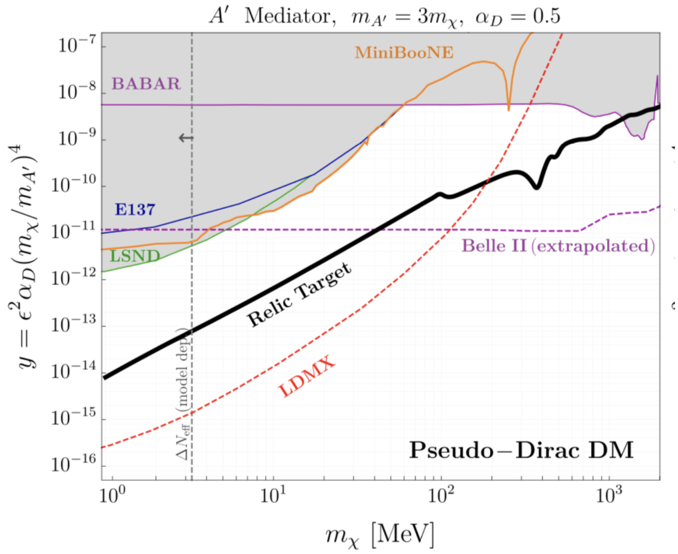

Figure 3.7: Light Dark Matter parameter space plotted in the yield variable plane, for pseudo-Dirac DM with dark coupling $\alpha_D = 0.5$, in conjunction with thermal relic target line. [69].

3.3 Relic abundance

The relic density depends directly on the annihilation rate of Dark Matter into normal matter, or the *self annihilation rate* $< \sigma_{ann} v >$, because this rate determines when it was, in the history of universal expansion, that Dark Matter decoupled from the thermal equilibrium at that point (Recall Fig. 2.1). Analytic expressions for the cross sections can again be determined from the Breit-Wigner distribution, and are given for different mediator types in [66]. We consider s-channel only because that corresponds to the leading order diagram for a single on-shell (non-virtual) mediator in the collision, and the corresponding expression is shown in Eq. 3.4.

$$\sigma^V_{\text{ann},s} \cdot v = \sum_q \frac{N_c^q g_{DM}^2 g_q^2 \beta_q}{2\pi} \frac{m_q^2 (4m_{DM}^2 - M_{med}^2)^2}{m_{med}^4 \left[(m_{med}^2 - 4m_{DM}^2)^2 + m_{med}^2 \Gamma_{med}^2 \right]} v^2 \tag{3.4}$$

Here, $N_c^q = 3$ is the *QCD color factor*, since there are 3 colors of quarks contributing, $\beta_q = \sqrt{1 - \frac{m_q^2}{m_{DM}^2}}$, and v is again the relative velocity of the annihilating DM.

Using this analytical approach to calculating the self annihilation rate, and therefore the relic density, allows for determination of the minimum allowed coupling value (g_q in Eq. 3.4) which leads to a value for the density compatible with what we observe. The entire mass-mass plane for m_{DM} and m_{med} can be visualized as a heat map, with coupling displayed on the z-axis, in order to conclude which regions in that plane could be relevant for the simplified models in question, based on an analysis of where the model can satisfy the relic density without overproducing DM.

By fixing the Dark Matter and mediator masses, m_{DM} and m_{med}, by assuming that coupling g_{DM} is a constant, and by observing that, from the Breit-Wigner distribution again, the decay width to Dark Matter $\Gamma_{DM} \propto g_{DM}^2$, Eq. 3.4 can be expressed as a quadratic equation in g_q^2. This leads to the conclusion that there is a well defined minimum in the relic density-coupling plane of $\Omega h^2 - g_q$, and two possible values of g_q that reproduce the relic density precisely. Any values of g_q below the minimum or above the maximum would overclose the universe, meaning too much Dark Matter would be produced to be accounted for by cosmological observation.

Figure 3.8 shows one example, from presentation slides belonging to Prof. Phil Harris (Massachusetts Institute of Technology), delivered for a dark sectors workshop at Brookhaven National Labs[71], for an axial-vector mediator. This is shown as a visual aid only. The minimum value of g_q corresponding to a value of Ωh^2 below the observed relic value boundary, represents the minimum allowed coupling corresponding to the model in question, and to the parameter configuration used. It is this value that is used for the z-axis on the heat maps shown in Figures 3.9 and 3.10.

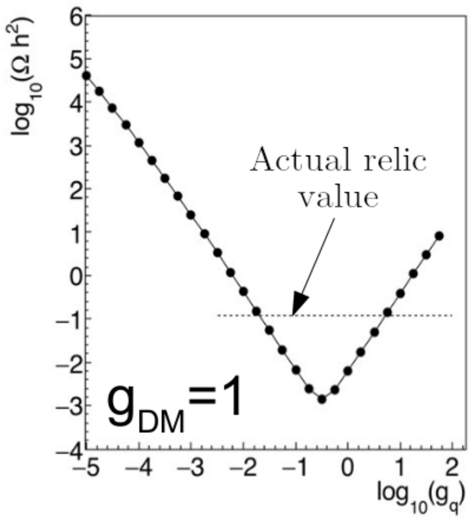

Figure 3.8: Quadratic relationship between thermal relic density Ωh^2 and SM coupling g_q, with Dark Matter coupling $g_{DM} = 1$, for an axial vector mediator. MadDM has been used to calculate each data point, and the observed relic value boundary has been imposed on the plot for clarity. [71]

The process to produce these plots is as follows: MadDM takes a mediator mass and a MadGraph model (e.g. DMSimp, HAHM) as inputs. For each mediator mass, it scans the mass range of all Dark Matter masses, selecting a pair of mass value at each point. For each mass pair, MadDM scans through either a range of g_q values if the model is DMSimp, or a range of ϵ values if the model is the HAHM model. It calculates the minimum value of g_q or ϵ for which the observed relic density is reproduced, corresponding to the leftmost data point beneath the relic line boundary in Figure 3.8. This value is color coded on the z-axis, and the whole mass-mass plane is presented as a heat map.

Figure 3.9 demonstrates that for light Dark Matter (< 50GeV) with a heavy vector mediator (500 to 2000 GeV), coloured dark orange and red on the figure, the lower limit on coupling is in the range of 1 to 10. Since this region requires larger couplings comparitively, in order not to overproduce, these mass combinations do not correspond to viable regions of the mass-mass parameter space. Very large coupling values, i.e. those > 1.0 have already been excluded.

For heavy Dark Matter (> 500 GeV) with a light mediator (< 500 GeV), there is a region where no solution was found to satisfy the cosmological relic density constraint. This corresponds to the white region on Figure 3.9.

There is a clearly visible resonant enhancement around the on-shell Breit-Wigner peak at $m_{med} \approx 2m_{DM}$, as one would expect. Here the minimum coupling value drops off the

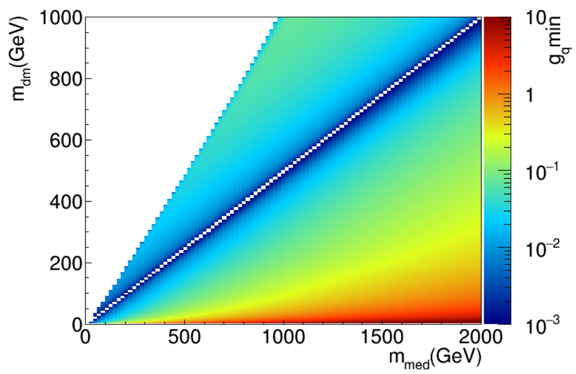

Figure 3.9: Minimum allowed coupling for the vector mediated model (DMSimp). The minimum coupling is computed on the z-axis.

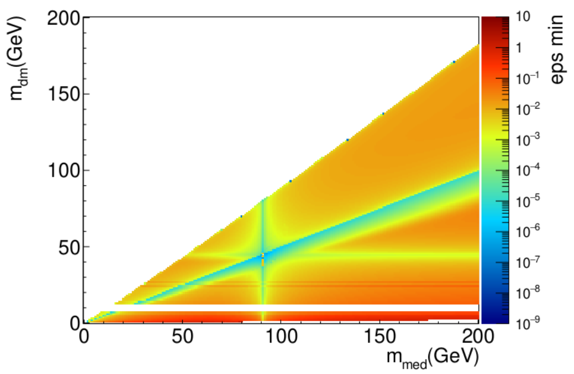

Figure 3.10: Minimum allowed Z mixing parameter ϵ for the dark photon mediated model (HAHM) with the Higgs decoupled. The minimum ϵ is computed on the z-axis.

scale of the z-axis, leading to the white diagonal line. Along this line, the resonance can occur much more easily, leading to a much lower limit on coupling to SM particles.

Also included is the lower mass range of the dark photon mediated HAHM model, Fig. 3.10; limited to the lower mass range because this is the only part of the parameter space which differs from the vector model in Figure 3.9. Again, the on-shell mediator enhancement is visible on the diagonal line where m_{DM} approaches $\frac{m_{med}}{2}$, but additionally, we now also have a resonant enhancement around the Z boson mass. This is due to the mixing between the dark photon Z' and the SM Z boson. When the mass of the dark photon mediator approaches the Z mass, the minimum mixing value drops substantially. This was seen also in Fig. 3.6 when the mediator mass approached the Z mass. The value of ϵ can be much lower for a dark photon close to the Z mass, since it becomes much easier for them to be produced along side on-shell Z bosons.

These bounds are valid only for these simplified models. They could change as more complications are introduced. For example, an interesting development to the dark photon model would be to re-introduce the dark Higgs, which would provide additional decay modes and mixing with the Standard Model Higgs. Again, this was excluded for this analysis since a simplified discussion around the effect of the Z mixing was desired.

4 Conclusion and outlook

4.1 Conclusions

In this thesis I have outlined the experimental frontiers as put forward by the Snowmass community effort, and identified the necessity for complementarity between frontiers in the search for Dark Matter. Minimal models are a versatile tool with which to conduct this search, and minimal dark photon benchmarks for thermal relic WIMP Dark Matter provide an illustrative focus for this subject, in particular for the comparison between sensitivity limits of the energy frontier at the LHC, and the intensity frontier exemplified primarily by LDMX in this paper.

Testing the simulated detector acceptances between different model parameters, in order to ensure the distribution shape did not change, was shown in Section 3.1 to allow for scaling between Dark Matter types without the need for further simulation. This test was also conducted between the vector mediated and dark photon mediated models used in the following Section 3.2.

The kinetic mixing mechanism inherent in dark photon models differs from a more general vector mediated model, which contains free couplings to the SM. Extending limits based on the last run of CMS data at the LHC, and then scaling those limits between these models has been demonstrated in Section 3.2, which allowed for a reduction in the need to simulate MC events across both models. Expected limits on both models, down to a mediator mass of 10GeV and in the context of the relic abundance for each model, from the LHC and the future HL-LHC, have been presented in Figure 3.6. Following this, I discussed the complementarity of the intensity frontier for masses below 10GeV (Figure 3.7).

The relic density plots shown in Figures 3.9 and 3.10, with their use of the z-axis heat map format, visually extend the usual way that the mass-mass plane is presented. (See Fig 5.3 in Appendix A). Fig 5.3[72] clearly shows the current exclusion regions from CMS for varying final states and complementary experimental approaches, but only for a fixed set of coupling parameters. It is essentially one 'slice' of what is displayed by the thermal relic heat map plots, which provide an additional visual representation of viable parameter space within each model.

Altogether this discussion has shown that complementarity clearly exists between energy and intensity frontiers. Having translated different simplified models to the same axis in Figure 3.6, complementarity and scalability between models has been demonstrated. This work has allowed for sensitivity comparison between HL-LHC limits (EF) and dark photon limits (IF/RF). An important conclusion is that the intensity frontier will be more sensitive at low mediator masses, complementary to the energy frontier. The calculated limits of this work will be added to the catalogue of Physics Beyond Colliders.

4.2 Outlook

An immediate extension to the work performed here, as alluded to earlier, would be to look at how the re-introduction of the dark Higgs into the HAHM dark photon model would have an effect on both the relic density, and the coupling sensitivites. The dark Higgs was decoupled in this investigation to isolate the effect of the Z Z' mixing in the most simple way possible. Recoupling the dark Higgs would cause mixing with the SM Higgs, as well as adding further mechanisms for the decay of the mediator. It would be interesting to analyze how this change would affect the observations made so far.

Another possible extension to this work would be to investigate how the dark photon constraints discussed could fit into models of dark showers searched for by ATLAS. Dark QCD refers to the possibility of a rich dark sector comprised of dark fermions that interact with each other through a new force analogous to the strong force of SM QCD. Dark quarks could dark-hadronize into dark jets, in a QCD-like parton shower within the dark sector itself. This dark sector could couple to the Standard Model through other specific portals, including a vector mediated interaction. There exists the potential for cross over from the preceeding discussion of dark photon benchmarks for minimal dirac fermion like Dark Matter, into constraints on such models. A related paper on this subject is [73].

Another European effort to facilitate cross discipline collaboration in particle physics is the European Science Cluster of Astronomy and Particle physics research infrastructures (ESCAPE) [74]. ESCAPE unites Astronomy, Astroparticle and Particle physics. With respect to Dark Matter specifically, there is recognition that the experiments within the ESCAPE infrastructure are relevant to complementarity of Dark Matter searches. To that end, the *Test Dark Matter Science Project* aims to exploit synergies between research communities in terms of data analysis and computing tools to continue connecting results from different experiments. The code associated with creating the plots and outputs of this report is directly in line with these goals, and will therefore be passed off to an undergraduate project at Lund University, as part of the ESCAPE Dark Matter project efforts.

The corresponding github repository, including all files required to reproduce the plot in Figs. 3.6, 3.9 and 3.10, can be found at: `https://github.com/josh-greaves/darkphoton`.

4.3 Experimental table

One final output of this work, also to be eventually shared with the iDMEU collective, is the beginning stages of a table of experiments relevent to minimal vector mediated benchmarks. This is shown in Figures 4.1 and 4.2. The table will be extended to include direct detection experiments outlined in the following sources: [75][76]

Name	Status Summary	Mass range (DM, A')	Source of mass range (reference)	Beam (type,energy)	Beam line / yield (fb, pot)	Homepage	TDR	Misc publications
BaBar	Ceased operation in 2008	10 MeV to 10 GeV	1406.298	PEP-II [SLAC] e- beam: 9GeV e+ beam: 3.1GeV	514 fb-1	https://babar.heprc.uvic.ca/	https://inspirehep.net/literature/	
Belle-II	Record setting instantaneous luminosity [June 2020]	10 MeV to GeV	2202.03452	√s = 10.58 GeV (ee KEKB collider)	50 ab-1	https://www.belle2.org/	https://arxiv.org/abs/1011.0352	
BES III	Operational	1 MeV to 1 GeV	1907.07046	√s up to 4.63 GeV	17 fb-1 (2011 to 2018)	http://bes3.ihep.ac.cn/	https://arxiv.org/abs/0911.4960	
LHCb	Fully operational - data collected during Run 2	0.1 to 100 GeV	1910.06926	14 TeV pp	5.5 fb-1 2016-2018	http://lhcb.web.cern.ch/	https://cds.cern.ch/record/2776	
ATLAS	Fully operational - limit data taken during runs 1 and 2	1 MeV to 55 GeV [Run 2] [Future] up to TeV	Phys. Rev. D 92, 092001	14 TeV pp	36.1 fb-1 LLP searches, 2015-2016 ~20 fb-1 Run 1	https://atlas.cern/	CERN-LHCC-2022-004 https://cds.cern.ch/record/2802 n	
CMS	Fully operational - data collected during Run 2	1 GeV to 500 GeV	2009.14009	14 TeV pp	130 fb-1 2016-2018	https://cms.cern/	https://cds.cern.ch/record/2759	
SeaQuest	Phase I data taking from 2018 to 2020 Currently operational	10 MeV to 10 GeV	1804.00661	Beam 120 GeV	1.44×10^8 POT (Phase I) 35 ab-1 (Phase I)	https://www.phy.anl.gov/mep/d	https://doi.org/10.1016/j.nima.2	
HPS	2019 and 2021 datasets being analyzed	20 MeV to 220 MeV	2203.08324	Beam 4.55 GeV (2019) Beam 3.74 GeV (2021)	122 pb-1 (30 days in 2019) 168 pb-1 (28 days in 2021)	-	1910.04886	
STCF (Super Tau Charm Factory)	Next generation e+ e- collider to take over from BES III. Implementing now to 2026	2 MeV to 1 GeV	1907.07046	√s up to 7 GeV	30 ab-1	-	-	

Figure 4.1: Experiments relevant to dark vector mediated benchmarks, for use at iDMEu. (1 of 2).

Name	Status Summary	Mass range (DM, A')	Source of mass range (reference)	Beam (type,energy)	Beam line / yield (fb, pot)	Homepage	TDR	Misc publications
LDMX	Design study/optimization phase	1 MeV to 1 GeV	1808.05219	8 (SLAC) - 16 (eSPS) GeV electrons	SLAC, Jefferson CEBAF, eSPS: 10^{16} - 10^{18} eot/yr	https://confluence.slac.stanford	-	https://arxiv.org
M3	Design study/optimization phase	1 MeV to 1 GeV	1804.03144	Fermilab Test beam facility FTBF: Phase 1 Mtest (15GeV) Phase 2 NM4 (15GeV muons)	10^{10}-10^{13} (mu)ot (phase 1 and 2)	-	-	https://arxiv.org
REDTOP	Proposal phase - aiming to run in 2023	1 MeV to 10 GeV	1910.08505	CERN PS 1.7GeV (eta) - 3.5 GeV(Eta')	PS: 10^{17} pot/yr yielding => 10^{13} eta/yr, 10^{11} eta'/yr	https://redtop.fnal.gov/	-	https://arxiv.org
NA64++	Taking data at H4 since 2016	1 MeV to 10 GeV	2021 status report: CERN-SPSC-2021-016 also PBC report also (2013)arXiv:1312.3309	H4 SPS (beam dump) (50-100 GeV electrons) M2 SPS (100-160GeV protons)	5x 10^{12} (Run 3) eot (6-8mths) 5x 10^{13} (Run 3) (mu)ot (1.5yrs)	https://na64.web.cern.ch/	-	https://na64.wel
NA62 ++	Run 2 data taking, proposal for Run 3	1 MeV to 10 GeV	Status reports 2018, 2019	CERN K12 SPS (400GeV protons)	3x10^{18} pot/yr (Run 3)	https://na62.web.cern.ch/	TDR: NA62-10-07 http://cds.cern.ch/record/14049	Status reports: https://na62.wel
AWAKE	Data taken during run 2. Further e- acceleration during 2021-24.	AWAKE is an experimental technique of electron acceleration using proton driven plasma wakefields. The technique could be used to supplement or improve electrons on target for experiments like NA64.	-	SPS (point 4) CNGS target hall (~50GeV electrons)	5x10^{9} e/bunch ~10^{16} eot/yr	https://awake.web.cern.ch/	TDR: CERN-SPSC-2013-013 ; SPSC-TDR-003 http://cds.cern.ch/record/15373	
SHiP	Aim to data take during Run 4 (HL-LHC 27-29) TDR for detector + facility by 2022 Construction 23-27	1 MeV to 1 GeV	TDR	SPS BDF(beam dump facility) (400GeV protons)	~4x10^{19} pot/yr	http://ship.web.cern.ch/	TDR: CERN-SPSC-2019-049 ; SPSC-SR-263 https://cds.cern.ch/record/2704	
FASER (FASER2)	LOI July 2018 Run 3 2022 (Run 4) data taking	0.01 GeV to 1 GeV	1811.12522	LHC (ATLAS) Service Tunnel TI12 (14 TeV protons)	3000 fb-1 pp	https://faser.web.cern.ch/	-	https://arxiv.org
MATHUSLA	Planned for Run 4 (HL LHC)	1 MeV to 10 GeV	1806.07396	Located ~60m above (transverse) ATLAS or CMS Interaction Point	3000 fb-1 pp	https://mathusla-experiment.we	-	https://mathusla
CODEX-b	Proposal phase - seeking funding. Aiming for HL-LHC. Proof of Concept (CODEX-beta) will demonstrate during Run 3	0.1 GeV to 20 GeV	1708.09395	LHC-b UXA hall, IP8 (14TeV pp)	300 fb-1 pp	-	-	
milliQan	2018 data collected by Demonstrator detector 33m frmo CMS Interaction Point. Funded for Run 3 data taking with 2 complementary detectors at CMS point P5.	10 MeV to 45 GeV [10 MeV to 80 GeV HL-LHC] *	2008.07877	CMS 14 TeV pp	200 fb-1 pp	-	-	
FerMINI	Proposal stage	10 MeV to 5 GeV *	1812.03998	120 GeV (FNAL main injector/recycler complex)	NuMI or LBNF/DUNE beamlines at FNAL (downstream) after pp collision on target; 10^{20}/10^{21} pot in 1 year (Respectively)	-	-	

Figure 4.2: Experiments relevant to dark vector mediated benchmarks, for use at iDMEu. (2 of 2).

5 Appendix A

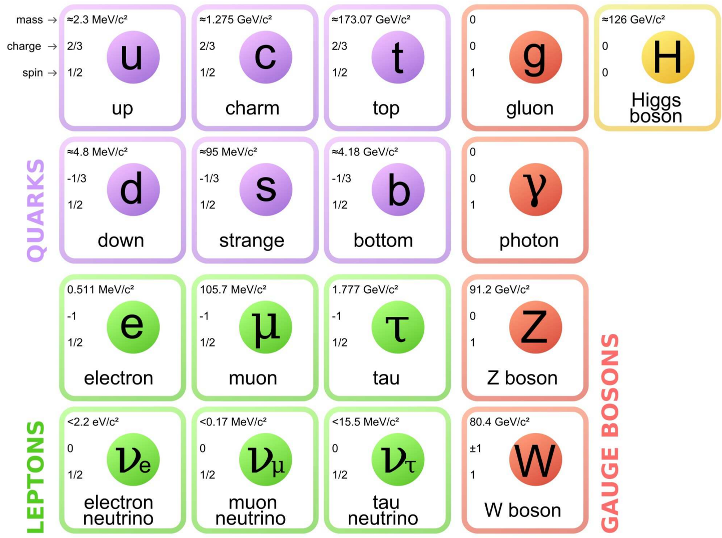

Figure 5.1: The fermions and bosons of the Standard Model.[77]

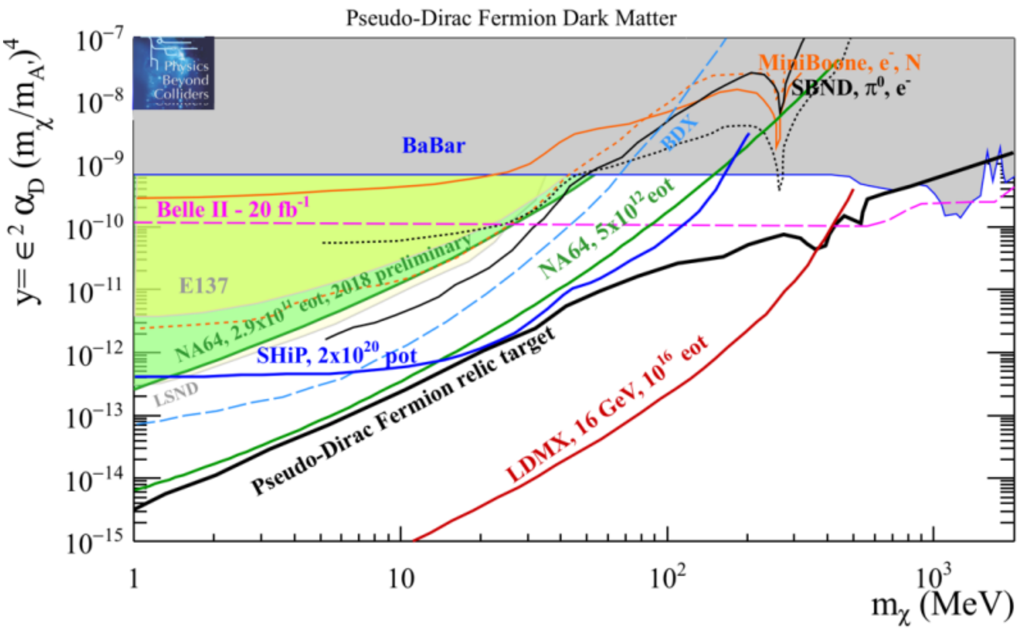

Figure 5.2: Dark Photon decaying to Pseudo-Dirac fermion. Prospective projects for Physics Beyond Colliders, on a timescale of 5 years (NA64 ++) and 10-15 years (LDMX, SHiP). Solid areas are currently excluded bounds, and the lines represent future experimental capabilities (solid) and projected capabilities (dashed). Assumptions are: dark coupling $\alpha_D = 0.1$ and $\frac{m_{A'}}{m_\chi} = 3$. Here the dark matter and mediator are refered to as m_χ and $m_{A'}$ respectively as opposed to m_{DM} and m_{med} in the rest of the text. [38].

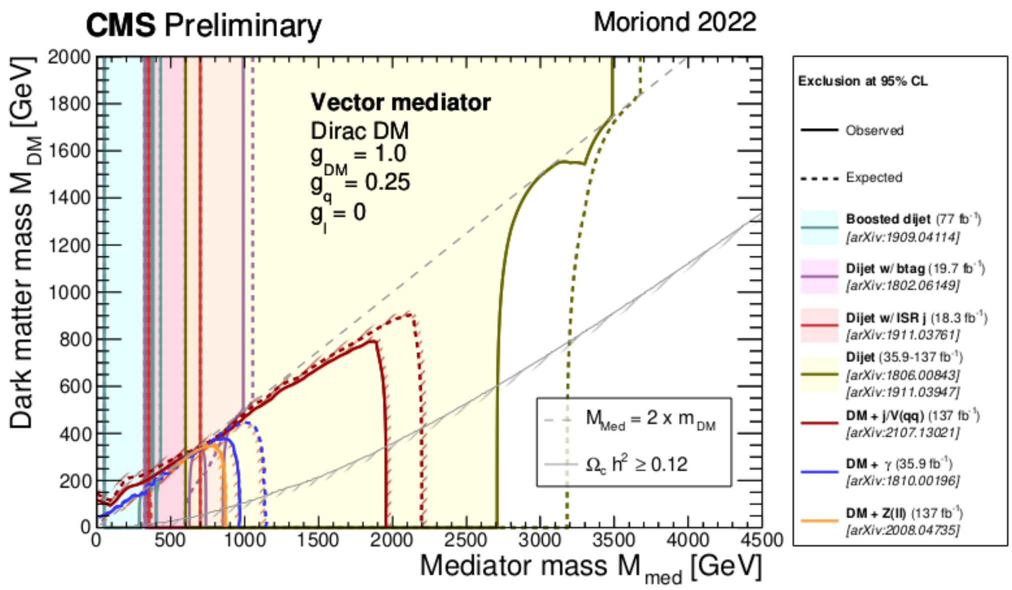

Figure 5.3: 95% CL observed and expected exclusion regions in mass-mass plane for vector mediated missing energy and di-jet final state searches from CMS. Couplings to leptons are $g_l = 0$. The assumed coupling parameters follow the directions of the DMWG [47] [66], and are set as $g_q = 0.25$ and $g_{DM} = 1.0$. [72].

References

[1] A. Pais and S. B. Treiman. "How Many Charm Quantum Numbers Are There?" In: *Phys. Rev. Lett.* 35 (1975), p. 1556. DOI: 10.1103/PhysRevLett.35.1556.

[2] Steven Weinberg. *World Science Festival 2015*. youtube. Accessed: 2022-2-18. 2015. URL: https://www.youtube.com/watch?v=g-y3DPJRVhE&t=435s.

[3] C. N. Yang and R. L. Mills. "Conservation of Isotopic Spin and Isotopic Gauge Invariance". In: *Phys. Rev.* 96 (1 1954), pp. 191–195. DOI: 10.1103/PhysRev.96.191. URL: https://link.aps.org/doi/10.1103/PhysRev.96.191.

[4] Peter W. Higgs. "Broken Symmetries and the Masses of Gauge Bosons". In: *Phys. Rev. Lett.* 13 (16 1964), pp. 508–509. DOI: 10.1103/PhysRevLett.13.508. URL: https://link.aps.org/doi/10.1103/PhysRevLett.13.508.

[5] F. Hoogeveen. "The standard model prediction for the electric dipole moment of the electron". In: *Nuclear Physics B* 341.2 (1990), pp. 322–340. ISSN: 0550-3213. DOI: https://doi.org/10.1016/0550-3213(90)90182-D. URL: https://www.sciencedirect.com/science/article/pii/055032139090182D.

[6] D. Hanneke, S. Fogwell, and G. Gabrielse. "New Measurement of the Electron Magnetic Moment and the Fine Structure Constant". In: *Physical Review Letters* 100.12 (2008). ISSN: 1079-7114. DOI: 10.1103/physrevlett.100.120801. URL: http://dx.doi.org/10.1103/PhysRevLett.100.120801.

[7] Brian Albert Robson. "The matter-antimatter asymmetry problem". In: *Journal of High Energy Physics, Gravitation and Cosmology* 04.01 (2018), 166–178. DOI: 10.4236/jhepgc.2018.41015.

[8] Christian Weinheimer and Kai Zuber. "Neutrino masses". In: *Annalen der Physik* 525.8-9 (2013), pp. 565–575. DOI: 10.1002/andp.201300063. URL: https://doi.org/10.1002%2Fandp.201300063.

[9] B. Abi et al. "Measurement of the Positive Muon Anomalous Magnetic Moment to 0.46 ppm". In: *Phys. Rev. Lett.* 126 (14 2021), p. 141801. DOI: 10.1103/PhysRevLett.126.141801. URL: https://link.aps.org/doi/10.1103/PhysRevLett.126.141801.

[10] Jack Dragos et al. "Confirming the existence of the strong CP problem in lattice QCD with the gradient flow". In: *Physical Review C* 103.1 (2021). DOI: 10.1103/physrevc.103.015202. URL: https://doi.org/10.1103%2Fphysrevc.103.015202.

[11] A Ashtekar and R Geroch. "Quantum theory of gravitation". In: *Reports on Progress in Physics* 37.10 (1974), pp. 1211–1256. DOI: 10.1088/0034-4885/37/10/001. URL: https://doi.org/10.1088/0034-4885/37/10/001.

[12] Michael Banks. "First black hole images unveiled". In: *Physics World* 32.5 (2019), pp. 8–10. DOI: 10.1088/2058-7058/32/5/9. URL: https://doi.org/10.1088/2058-7058/32/5/9.

[13] Abbott B. P. and Abbott R. et al. "Observation of Gravitational Waves from a Binary Black Hole Merger". In: *Physical Review Letters* 116.6 (2016). ISSN: 1079-7114. DOI: 10.1103/physrevlett.116.061102. URL: http://dx.doi.org/10.1103/PhysRevLett.116.061102.

[14] Heinz Andernach and Fritz Zwicky. *English and Spanish Translation of Zwicky's (1933) The Redshift of Extragalactic Nebulae*. 2017. arXiv: 1711.01693 [astro-ph.IM].

[15] E. Ward and ATLAS Collaboration and others. "Percentage of ordinary matter, dark matter and dark energy in the universe, as measured by the Planck satellite." In: (2019). URL: https://atlas.cern/updates/feature/dark-matter.

[16] Planck Collaboration, Ade, P. A. R., and Aghanim, N. et al. "Planck 2013 results. I. Overview of products and scientific results". In: *A&A* 571 (2014), A1. DOI: 10.1051/0004-6361/201321529. URL: https://doi.org/10.1051/0004-6361/201321529.

[17] V.C. Rubin, Jr. Ford W.K., and N. Thonnard. "Rotational properties of 21 SC galaxies with a large range of luminosities and radii, from NGC 4605 (R=4kpc) to UGC 2885 (R=122kpc)." In: *apj* 238 (June 1980), pp. 471–487. DOI: 10.1086/158003.

[18] Joel Primack. "Dark Matter and Galaxy Formation". In: 1192 (Sept. 2009). DOI: 10.1063/1.3274198.

[19] Douglas Clowe et al. "A Direct Empirical Proof of the Existence of Dark Matter". In: *The Astrophysical Journal* 648.2 (2006), pp. L109–L113. DOI: 10.1086/508162. URL: https://doi.org/10.1086/508162.

[20] Xiang-Ping Wu et al. "A comparison of different cluster mass estimates: consistency or discrepancy?" In: *Monthly Notices of the Royal Astronomical Society* 301.3 (1998), pp. 861–871. DOI: https://doi.org/10.1046/j.1365-8711.1998.02055.x. eprint: https://onlinelibrary.wiley.com/doi/pdf/10.1046/j.1365-8711.1998.02055.x. URL: https://onlinelibrary.wiley.com/doi/abs/10.1046/j.1365-8711.1998.02055.x.

[21] G. L. Bayatian et al. "CMS Physics: Technical Design Report Volume 1: Detector Performance and Software". In: CERN Document Server: CERN-LHCC-2006-001, CMS-TDR-8-1 (2006).

[22] LHC. *Large Hadron Collider*. Accessed: 2022-5-11. URL: https://home.cern/science/accelerators/large-hadron-collider.

[23] Torsten Åkesson et al. *Light Dark Matter eXperiment (LDMX)*. 2018. DOI: 10.48550/ARXIV.1808.05219. URL: https://arxiv.org/abs/1808.05219.

[24] A. Airapetian et al. “ATLAS: Detector and physics performance technical design report. Volume 1”. In: CERN Document Server: CERN-LHCC-99-14, ATLAS-TDR-14 (May 1999).

[25] Martina Pili. “Performance of the LHCb detector in the Run 2”. In: *PoS* ICHEP2020 (2021), 767. 6 p. DOI: 10.22323/1.390.0767. URL: https://cds.cern.ch/record/2783948.

[26] P Cortese et al. “ALICE: Physics performance report, volume I”. In: *J. Phys. G* 30 (2004). Ed. by F Carminati et al., pp. 1517–1763. DOI: 10.1088/0954-3899/30/11/001.

[27] The ATLAS Collaboration. “Search for new phenomena in events with an energetic jet and missing transverse momentum in p p collisions at $\sqrt{s} = 13$TeV with the ATLAS detector”. In: *Physical Review D* 103.11 (2021). DOI: 10.1103/physrevd.103.112006. URL: https://doi.org/10.1103%2Fphysrevd.103.112006.

[28] CMS Collaboration. “Search for new particles in events with energetic jets and large missing transverse momentum in proton-proton collisions at $\sqrt{s} = 13$ TeV”. In: *Journal of High Energy Physics* 2021.11 (2021). DOI: 10.1007/jhep11(2021)153. arXiv: 2107.13021.

[29] Sergey Alekhin et al. *IOP Rep. Prog. Phys. 79 124201*. 2016.

[30] Rouven Essig. *The low-mass dark matter frontier*. 2020. URL: https://physics.aps.org/articles/v13/172.

[31] American Physical Society. *Snowmass DPF community planning exercise*. 2020. URL: https://snowmass21.org/.

[32] Rebeca Gonzalez Suarez. *The Future Circular Collider (FCC) at CERN*. 2022. DOI: 10.48550/ARXIV.2204.10029. URL: https://arxiv.org/abs/2204.10029.

[33] Ackermann M. et al. “Dark matter constraints from observations of 25 Milky Way satellite galaxies with the Fermi Large Area Telescope”. In: *Phys. Rev. D* 89 (4 2014), p. 042001. DOI: 10.1103/PhysRevD.89.042001. URL: https://link.aps.org/doi/10.1103/PhysRevD.89.042001.

[34] C. Doglioni. *Schematic illustration of Dark Matter (DM) interactions and their corresponding experimental detection techniques*. 2019. URL: https://cds.cern.ch/record/2665196.

[35] Andreas Albert, Antonio Boveia, Josh Greaves, et al. *Displaying dark matter constraints from colliders with varying simplified model parameters*. 2022. DOI: 10.48550/ARXIV.2203.12035. URL: https://arxiv.org/abs/2203.12035.

[36] Antonio Boveia, Caterina Doglioni, et al. *Summarizing experimental sensitivities of collider experiments to dark matter models and comparison to other experiments*. 2022. DOI: 10.48550/ARXIV.2206.03456. URL: https://arxiv.org/abs/2206.03456.

[37] Batell B. et al. *Dark Matter Complementarity*. 2022. DOI: To_be_published_soon.

[38] J Beacham et al. "Physics beyond colliders at CERN: beyond the Standard Model working group report". In: *Journal of Physics G: Nuclear and Particle Physics* 47.1 (2019), p. 010501. DOI: 10.1088/1361-6471/ab4cd2. URL: https://doi.org/10.1088%2F1361-6471%2Fab4cd2.

[39] C. Doglioni et al. JENAS 2019. *initiative for Dark Matter in Europe and beyond*. 2019. URL: https://idmeu.org/.

[40] Adam Green. *Dark Matter Freeze Out: An Origin Story*. 2020. URL: https://www.particlebites.com/?p=7004.

[41] E Kolb and M Turner. *The early universe*. Addison-Wesley, 1994.

[42] Jonathan L Feng, Huitzu Tu, and Hai-Bo Yu. "Thermal relics in hidden sectors". In: *Journal of Cosmology and Astroparticle Physics* 2008.10 (2008), p. 043. DOI: 10.1088/1475-7516/2008/10/043. URL: https://doi.org/10.1088%2F1475-7516%2F2008%2F10%2F043.

[43] S. D. M. White, C. S. Frenk, and M. Davis. "Clustering in a neutrino-dominated universe". In: *apjl* 274 (Nov. 1983), pp. L1–L5. DOI: 10.1086/184139.

[44] Miguel Zumalacárregui and Uro š Seljak. "Limits on Stellar-Mass Compact Objects as Dark Matter from Gravitational Lensing of Type Ia Supernovae". In: *Phys. Rev. Lett.* 121 (14 2018), p. 141101. DOI: 10.1103/PhysRevLett.121.141101. URL: https://link.aps.org/doi/10.1103/PhysRevLett.121.141101.

[45] R. D. Peccei and Helen R. Quinn. "CP Conservation in the Presence of Pseudoparticles". In: *Phys. Rev. Lett.* 38 (25 1977), pp. 1440–1443. DOI: 10.1103/PhysRevLett.38.1440. URL: https://link.aps.org/doi/10.1103/PhysRevLett.38.1440.

[46] Daniel Abercrombie and Nural Akchurin et al. "Dark Matter benchmark models for early LHC Run-2 Searches: Report of the ATLAS/CMS Dark Matter Forum". In: *Physics of the Dark Universe* 27 (2020), p. 100371. ISSN: 2212-6864. DOI: https://doi.org/10.1016/j.dark.2019.100371. URL: https://www.sciencedirect.com/science/article/pii/S2212686419301712.

[47] Antonio Boveia et al. *Recommendations on presenting LHC searches for missing transverse energy signals using simplified s-channel models of dark matter*. 2016. DOI: 10.48550/ARXIV.1603.04156. URL: https://arxiv.org/abs/1603.04156.

[48] Paul A. M. Dirac. "The quantum theory of the electron". In: *Proc. Roy. Soc. Lond. A* 117 (1928), pp. 610–624. DOI: 10.1098/rspa.1928.0023.

[49] David Curtin et al. "Illuminating dark photons with high-energy colliders". In: *Journal of High Energy Physics* 2015.2 (2015). DOI: 10.1007/jhep02(2015)157. URL: https://arxiv.org/abs/1412.0018.

[50] Marco Fabbrichesi, Emidio Gabrielli, and Gaia Lanfranchi. *The Physics of the Dark Photon*. Springer International Publishing, 2021. DOI: 10.1007/978-3-030-62519-1. URL: https://doi.org/10.1007%2F978-3-030-62519-1.

[51] Hooman Davoudiasl, Hye-Sung Lee, and William J. Marciano. "Dark Z implications for parity violation, rare meson decays, and Higgs physics". In: *Physical Review D* 85.11 (2012). DOI: 10.1103/physrevd.85.115019. URL: https://doi.org/10.1103%2Fphysrevd.85.115019.

[52] Lee Hye-Sung. *Physics of Dark Z boson, Hye-Sung Lee [presentation slides]*. CERN theory group retreat 2014, Les Houches Centre de Physique. 2014. URL: https://www.houches-school-physics.com/program/program-2014/.

[53] J. Alwall et al. "The automated computation of tree-level and next-to-leading order differential cross sections, and their matching to parton shower simulations". In: *Journal of High Energy Physics* 2014.7 (2014). DOI: 10.1007/jhep07(2014)079. URL: https://doi.org/10.1007%2Fjhep07%282014%29079.

[54] Torbjörn Sjöstrand et al. "An introduction to PYTHIA 8.2". In: *Computer Physics Communications* 191 (2015), pp. 159–177. DOI: 10.1016/j.cpc.2015.01.024. URL: https://doi.org/10.1016%2Fj.cpc.2015.01.024.

[55] Eric Conte, Benjamin Fuks, and Guillaume Serret. "MadAnalysis 5, a user-friendly framework for collider phenomenology". In: *Computer Physics Communications* 184.1 (2013), pp. 222–256. DOI: 10.1016/j.cpc.2012.09.009. URL: https://doi.org/10.1016%2Fj.cpc.2012.09.009.

[56] S. Ovyn, X. Rouby, and V. Lemaitre. *Delphes, a framework for fast simulation of a generic collider experiment*. 2009. DOI: 10.48550/ARXIV.0903.2225. URL: https://arxiv.org/abs/0903.2225.

[57] Christian Bierlich and Andy Buckley et al. "Robust Independent Validation of Experiment and Theory: Rivet version 3". In: *SciPost Physics* 8.2 (2020). DOI: 10.21468/scipostphys.8.2.026. URL: https://doi.org/10.21468%2Fscipostphys.8.2.026.

[58] Enrico Bothmann et al. "Event generation with Sherpa 2.2". In: *SciPost Physics* 7.3 (2019). DOI: 10.21468/scipostphys.7.3.034. URL: https://doi.org/10.21468%2Fscipostphys.7.3.034.

[59] B. Andersson et al. "Parton fragmentation and string dynamics". In: *Physics Reports* 97.2 (1983), pp. 31–145. ISSN: 0370-1573. DOI: https://doi.org/10.1016/0370-1573(83)90080-7. URL: https://www.sciencedirect.com/science/article/pii/0370157383900807.

[60] L. Lönnblad and T. Sjöstrand. *Theoretical particle physics - Strong Interactions [Lecture slides]*. Institutionen för Astronomi och teoretisk fysik, Lunds Universitet. Feb. 2020. URL: "http://home.thep.lu.se/fytn04/".

[61] ATLAS collaboration. "Search for new phenomena in final states with an energetic jet and large missing transverse momentum in p p collisions at $\sqrt{s} = 13$TeV using the ATLAS detector". In: *Physical Review D* 94.3 (2016). DOI: 10.1103/physrevd.94.032005. URL: https://doi.org/10.1103%2Fphysrevd.94.032005.

[62] TASSO collaboration. "Evidence for planar events in ee annihilation at high energies". In: *Physics Letters B* 86.2 (1979), pp. 243–249. ISSN: 0370-2693.

[63] Adam Alloul and Neil D. Christensen et al. "FeynRules 2.0 — A complete toolbox for tree-level phenomenology". In: *Computer Physics Communications* 185.8 (2014), pp. 2250–2300. DOI: 10.1016/j.cpc.2014.04.012. URL: https://doi.org/10.1016%2Fj.cpc.2014.04.012.

[64] Kentarou Mawatari. *Feynrules madgraph model: DMsimp spin-0*. Version 1.0. Mar. 25, 2018. URL: http://feynrules.irmp.ucl.ac.be/wiki/DMsimp.

[65] David Curtin, Rouven Essig, et al. "Exotic decays of the 125 GeV Higgs boson". In: *Phys. Rev. D* 90 (7 2014), p. 075004. DOI: 10.1103/PhysRevD.90.075004. URL: https://link.aps.org/doi/10.1103/PhysRevD.90.075004.

[66] Andreas Albert, Mihailo Backovic, Antonio Boveia, et al. *Recommendations of the LHC Dark Matter Working Group: Comparing LHC searches for heavy mediators of dark matter production in visible and invisible decay channels*. 2017. DOI: 10.48550/ARXIV.1703.05703.

[67] Eder Izaguirre et al. "Analyzing the Discovery Potential for Light Dark Matter". In: *Physical Review Letters* 115.25 (2015). DOI: 10.1103/physrevlett.115.251301. URL: https://doi.org/10.1103%2Fphysrevlett.115.251301.

[68] G Apollinari et al. *High Luminosity Large Hadron Collider HL-LHC*. en. 2015. DOI: 10.5170/CERN-2015-005.1. URL: https://cds.cern.ch/record/2120673.

[69] Asher Berlin et al. "Dark matter, millicharges, axion and scalar particles, gauge bosons, and other new physics with LDMX". In: *Physical Review D* 99.7 (2019). DOI: 10.1103/physrevd.99.075001.

[70] European Strategy For Particle Physics Preparatory Group. *Physics Briefing Book*. 2019. DOI: 10.48550/ARXIV.1910.11775.

[71] Philip Harris. *Dark Matter Mediators @ Colliders [presentation slides]*. Dark Interactions: Perspectives from Theory and Experiment. 2018. URL: https://www.bnl.gov/di2018/.

[72] CMS Collaboration. "CMS Exotica Summary plots for 13 TeV data". In: 2022 (2022). URL: twiki.cern.ch/twiki/bin/view/CMSPublic/SummaryPlotsEXO13TeV.

[73] Nicoline Hemme. "Studies of Dark Showers for Present and Future Colliders". In: (2022). DOI: DOItobepublishedsoon. arXiv: DOItobepublishedsoon [hep-ex].

[74] Mark G. Allen et al. *ESCAPE – addressing Open Science challenges*. 2020. DOI: 10.48550/ARXIV.2012.11534. URL: https://arxiv.org/abs/2012.11534.

[75] Rouven Essig et al. *Snowmass2021 Cosmic Frontier: The landscape of low-threshold dark matter direct detection in the next decade*. 2022. DOI: 10.48550/ARXIV.2203.08297. URL: https://arxiv.org/abs/2203.08297.

[76] J. R. Angevaare et al. "Complementarity of direct detection experiments in search of light Dark Matter". In: *arXiv e-prints* (Apr. 2022). arXiv: 2204.01580 [hep-ph].

[77] User:MissMJ, Public Domain. *'File:Standard Model of Elementary Particles.svg'*. https://commons.wikimedia.org/wiki/File:Standard_Model_of_Elementary_Particles.svg. Own work uploaded User; Online; accessed 11-May-2022.